SMOS disaggregated soil moisture product at 1 km resolution

B. Molero, O. Merlin, Y. Malbéteau, A. Al Bitar, F. Cabot, V. Stefan, Y. Kerr, S. Bacon, M.H. Cosh, R. Bindlish, et al.

To cite this version:

B. Molero, O. Merlin, Y. Malbéteau, A. Al Bitar, F. Cabot, et al.. SMOS disaggregated soil moisture product at 1 km resolution: Processor overview and first validation results. Remote Sensing of Environment, 2016, 180, pp.361-376. 10.1016/j.rse.2016.02.045 . hal-03834583

HAL Id: hal-03834583
https://hal.science/hal-03834583

Submitted on 30 Oct 2022

SMOS disaggregated soil moisture product at 1 km resolution: processor overview and first validation results

B. Molero[1]*, O. Merlin[1, 2], Y. Malbéteau[1], A. Al Bitar[1], F. Cabot[1],
V. Stefan[1], Y. Kerr[1], S. Bacon[1], M. H. Cosh[3], R. Bindlish[3], T. J. Jackson[3]

1 Centre d'Etudes Spatiales de la Biosphère, Toulouse, France
2 Université Cadi Ayyad, Marrakech, Morocco
3 USDA ARS Hydrology and Remote Sensing Laboratory, USA
* beatriz.molero@cesbio.cnes.fr; tel.: +33 5 61 55 74 87

Keywords: disaggregation, soil moisture, processor, SMOS, CATDS, Level 4

Abstract: The SMOS (Soil Moisture and Ocean Salinity) mission provides surface soil moisture (SM) maps at a mean resolution of ~50 km. However, agricultural applications (irrigation, crop monitoring) and some hydrological applications (floods and modeling of small basins) require higher resolution SM information. In order to overcome this spatial mismatch, a disaggregation algorithm called Disaggregation based on Physical And Theoretical scale Change (DISPATCH) combines higher-resolution data from optical/thermal sensors with the SM retrieved from microwave sensors like SMOS, producing higher-resolution SM as the output. A DISPATCH-based processor has been implemented for the whole globe (emerged lands) in the Centre Aval de Traitement des Données SMOS (CATDS), the French data processing center for SMOS Level 3 products. This new CATDS Level-4 Disaggregation processor (C4DIS) generates SM maps at 1 km resolution. This paper provides an overview of the C4DIS architecture, algorithms and output products. Differences with the original DISPATCH prototype are explained and major processing parameters are presented. The C4DIS SM product is compared against L3 and *in situ* SM data during a one year period over the Murrumbidgee catchment and the Yanco area (Australia), and during a four and a half year period over the Little Washita and the Walnut Gulch watersheds (USA). The four validation areas represent highly contrasting climate regions with different landscape properties. According to this analysis, the C4DIS SM product improves the spatio-temporal correlation with *in situ* measurements in the semi-arid regions with substantial SM spatial variability mainly driven by precipitation and irrigation. In sub-humid regions like the Little Washita watershed, the performance of the algorithm is poor except for summer, as result of the weak moisture-evaporation coupling. Disaggregated products do not succeed to have and additional benefit in the Walnut Gulch watershed, which is also semi-arid but with well-drained soils that are likely to cancel the spatial contrast needed by DISPATCH. Although further validation studies are still needed to better assess the performance of DISPATCH in a range of surface and atmospheric conditions, the new C4DIS product is expected to provide satisfying results over regions having medium to high SM spatial variability.

1. Introduction

Soil moisture (SM) is an essential component of the water cycle that impacts infiltration, runoff and evaporation processes. In addition, it modulates the energy exchange as well as the carbon exchange at the land surface (Daly & Porporato, 2005). SM has influence over a range of spatial scales: the climatic (Douville, 2004; Laio et al., 2002), the meteorological (Dirmeyer, 2000; Drusch, 2007), the hydrological (Chen et al., 2011; Draper et al., 2012), the parcel and the local scale (Guérif & Duke, 2000).

Current satellite missions provide surface SM observations at large scales on a global basis. Passive microwave L-band observations are widely used for surface SM retrievals, but in practice they constrain the resolution of the retrievals to 30-60 km (Kerr & Njoku, 1990; Njoku & Entekhabi, 1996; Schmugge, 1998) with current technology. The Soil Moisture Ocean Salinity (SMOS) mission, launched in November 2009, incorporates an interferometric radiometer at L-band (1.4 GHz) and provides SM with a resolution of 30-55 km and a sensing depth of 3-5 cm (Kerr et al., 2001, 2010). SMOS Level 2 (L2) and Level 3 (L3) SM products have been validated extensively on a regular basis since the beginning of the mission (Al Bitar et al., 2012; Delwart et al., 2008) and they have been assessed as suitable for hydro-climate applications (Lievens et al., 2015; Wanders et al., 2014). However, most hydro-agricultural applications need SM measurements of sub-kilometer spatial resolution with a still representative temporal coverage (Walker & Houser, 2004). We should strive to provide a high resolution (HR) SM product that would enhance the knowledge of the hydrological processes at local scale.

Different satellite-based approaches have been proposed to retrieve SM. One of the most popular is the use of active sensors like the synthetic aperture radars (SAR) (ERS, ALOS, Sentinel 1) or scatterometers (ASCAT). These instruments provide observations with a variety of spatial and time resolutions but they are influenced to a great extent by the scattering produced by vegetation structure and surface roughness, among other factors. Unlike active sensors, passive instruments are much less sensitive to scattering but provide surface SM estimations at coarse resolutions (>40 km). C- and X-band radiometers like AMSR-E and WindSat have shown good results (Mladenova et al., 2011), but because of the frequency used, their sensing depth is shallow (~1cm) and vegetation becomes rapidly opaque. In contrast, L-band radiometer acquisitions from SMOS provide SM estimations for a much wider range of vegetation conditions, with a sensing depth of around 5 cm and a revisit time of ~3 days. However, the spatial resolution provided is also coarse (35-55 km) as mentioned previously. The main strategies to workaround this issue while maintaining the benefits of L-band consist of merging the L-band acquisitions with HR ancillary data, namely radar and optical observations.

Over the past decade, various methods have been proposed to combine active and passive sensors to produce HR SM (Das et al., 2011; Narayan et al., 2006; Zhan et al., 2006). The NASA Soil Moisture Active Passive (SMAP) mission, launched in 2015, intended to combine L-band brightness temperatures (TB) and HR L-band radar backscatter data (Entekhabi et al., 2010a). Despite the radar failure in July 2015, related previous studies showed that SM could have been delivered at 9 km and even 3 km resolution (Das et al., 2014).

Optical sensors (visible/near-infrared/thermal-infrared) can achieve finer spatial resolutions. However, the quality of their observations is critically compromised by the presence of clouds. Examples of optical sensors include the Landsat instruments and the Advanced Spaceborne Thermal Emission and Reflection radiometer (ASTER), with data at ~100 m resolution, and the MODerate resolution Imaging Spectroradiometer (MODIS), with data at ~1 km resolution. Such data include soil temperature and vegetation cover information, which are variables linked to soil water content (Fang et al., 2013). The relationship between land surface temperature (LST) and normalized difference vegetation index (NDVI) was first formalized in the 90s with the triangle (Carlson et al., 1994; Carlson, 2007) and the trapezoid (Moran et al., 1994) approaches.

Most of the methods for deriving HR SM from the synergy between optical and microwave observations are based on the triangle/trapezoid approaches. Chauhan et al. (2003) stated that the relationship between LST, NDVI and SM can be formulated as a regression formula specific to the region and climatic conditions. Later, Piles et al. (2011) included SMOS TBs in the equation, which reduced the bias but slightly degraded the spatio-temporal correlation between the obtained HR SM and the *in situ* measurements. These empirical methods need local calibration of the regression coefficients at low resolution (LR) before applying them to the HR ancillary data. On the contrary, semi-physical methods replace the polynomial function by physically-based models that use evaporation as a proxy variable for SM variability. Merlin et al. (2008) linked the SM to the soil evaporative efficiency (SEE), defined as the ratio of actual to potential soil evaporation. Kim & Hogue (2012) established a linear relationship between the soil evaporative fraction of Jiang & Islam (2003) and SM. Both approaches improved the satellite SM spatial variability and showed better correspondence with ground measurements in the area of study (SMEX04).

The semi-physical methods have three important advantages with respect to the purely empirical methods: (i) the mean SM is preserved across the merging process (which justifies calling it 'disaggregation' or 'downscaling'), (ii) a physical link is established for HR between SM and the evaporation/evapotranspiration rate and (iii) no local calibration or fit is needed. These are key factors in developing a robust and global operational algorithm for HR SM.

Recent studies by Merlin et al. (2012, 2013) have improved the evaporation rate calculation and the evaporation-SM link of Merlin et al. (2008). The DISaggregation based on Physical And Theoretical scale Change (DISPATCH) algorithm estimates SEE at high-resolution from soil temperature and vegetation data for modeling the spatial variations inside the microwave SM observation. In Merlin et al. (2012), DISPATCH included corrections for the microwave sensor weighting function and grid oversampling and provided an estimate of the uncertainty in the output disaggregated data. Later, Merlin et al. (2013) demonstrated that the linear approximation of the SEE-SM link model is suitable for kilometer scales and included soil temperature corrections for elevation effects. Both studies were conducted under semi-arid conditions, in a 500x100 km study area within the Murrumbidgee river catchment, in southeastern Australia, and in a 60x60 km study area east of Lleida in Catalunya, Spain. They showed that DISPATCH improves the spatio-temporal correlation with *in situ* measurements, but that the accuracy of disaggregated products is highly dependant on the SM-evaporation coupling. The downscaled resolution of 1 km (Merlin et al., 2009, 2013) and the combination of satellite data from different time stamps in DISPATCH (Malbéteau et al., 2016b; Merlin et al., 2012) have been considered as a good trade-off between spatial representativeness and overall accuracy, given the current status of the algorithm.

Recently, a new Level-4 (L4) processor (C4DIS) based on DISPATCH has been implemented in the Centre Aval de Traitement des Données SMOS (CATDS), the French ground segment for SMOS Level-3 and Level-4 data. The aim is to disaggregate the SMOS CATDS Level-3 (L3) 1-day SM maps to produce maps of SM at 1 km resolution for any part of the globe on an operational basis. The ancillary temperature and vegetation data are retrieved from the MODIS mission.

This paper seeks (i) to provide an overview of the C4DIS architecture, processing algorithms, output products, strengths and weaknesses and (ii) to derive the first conclusions on the performance of the C4DIS product depending on the climatic and landscape conditions. To do so, we evaluate the C4DIS product against *in situ* data from the Murrumbidgee catchment and two additional contrasting networks. Former versions of DISPATCH have so far been evaluated mostly in semi-arid conditions (Merlin et al., 2012, 2013, Malbéteau et al., 2015). The Murrumbidgee network belongs to these previous studies, and it is included here to serve as a reference for the current version of DISPATCH and the C4DIS processor and for the other validation areas. The two other *in situ* networks considered in this study are located in the Little Washita watershed in Oklahoma, USA, which exhibits sub-humid conditions, and the Walnut Gulch watershed in Arizona, USA, which exhibits semi-arid to arid conditions. Their relief, soil properties and land use differ from the Murrumbidgee's. The L4 disaggregated SM product is evaluated using *in situ* 0–5 cm and *in situ* 0–8 cm measurements taken at the same time as SMOS overpasses (around 6 am, 6 pm) during the period 01/06/2010 to 31/05/2011 for the Australian network and 01/06/2010 to 31/12/2014 for the USA networks. These networks have been providing ground SM data in a continuous basis and have contributed to the validation of different satellite missions, SMOS among them (Cosh et al., 2004; Jackson et al., 2010, 2012; Leroux et al., 2013; Peischl et al., 2012).

It is important to note that the DISPATCH algorithm will continue to evolve. Validation activities on the Level-4 processor C4DIS will provide valuable information for the improvement of the algorithm and processing chain. This current study is conducted on the products of the first version of the C4DIS processor.

2. Input data collection

2.1 In situ measurements

Three validation networks were selected for this work, the Murrumbidgee Soil Moisture Monitoring Network (MB) in Australia (Smith et al., 2012) and two different USDA (United Stated Department of Agriculture) networks: Little Washita (LW) in Oklahoma (Cosh et al., 2006) and Walnut Gulch (WG) in Arizona (Cosh et al., 2008). They exhibit contrasted types of climate, soil properties, land use and spatial extension.

The MB network covers a large extension (82,000 km^2) in southern New South Wales. Its climate ranges from semi-arid in the west (average annual precipitation of 300 mm), to humid in the east (annual precipitation of 1900 mm at the Snowy Mountains). The MB has been studied in previous DISPATCH campaigns (Malbéteau et al., 2016b; Merlin et al., 2012). It is included here for different reasons: it permits to confront results with previous versions of the algorithm, it contains within the Yanco area, which gathers the nominal landscape and climatic conditions for DISPATCH (flat, semi-arid with low vegetation), and it shows a variety of climate, soil and land use cases that can reveal the usefulness of disaggregation.

The MB consists in 38 validation stations: 18 of them provide SM integrated over the first 8 cm of soil (Campbell Scientific water content reflectometers) and the rest provide SM integrated over the first 5 cm of soil (Stevens Hydra Probe). The stations are situated in four areas: 7 stations in the limits of the catchment near to regional centers; 5 stations in Adelong Creek (145 km^2), a grazing area with steep slopes; 13 stations in Kyeamba creek (600 km^2), a catchment with gentle slopes and grazing and dairy land use; and finally, 13 stations in the Yanco region (3000 km^2).

Yanco soils are mainly silty-loam. The climate is semi-arid with an average annual rainfall of about 400 mm, with most of the precipitation occurring in winter and spring. The land use is divided into irrigation and dry land cropping and pastures. This area has been extensively monitored since 2001 (Smith et al.,

2012) and has been used in a variety of satellite validation campaigns (Mladenova et al., 2011; Panciera et al., 2014; Peischl et al., 2012)

The USDA networks have been operating since 2002 and they have been used in the validation of Advanced Microwave Scanning Radiometer-Earth Observing System (AMSR-E) products (Jackson et al., 2010), Aquarius (Bindlish, 2015), ASCAT (Leroux et al., 2013) and SMOS products (Jackson et al., 2012). The probes are installed at a depth of 5 cm, with an effective measurement depth between 3 and 7 cm (Stevens Hydra Probe).

LW is located in southwest Oklahoma and covers an area of about 610 km^2. The climate is sub-humid with an average annual rainfall of 750 mm. Summers are hot and relatively dry while winters are short and temperate. Autumn and spring are when most of the precipitation occurs (Allen & Naney, 1991). The land use is mainly rangeland and crops that include winter wheat and some corn and grasses. Soils include a wide range of textures, with large regions of sands, loams and clays. The topography is moderately rolling with few hills.

WG occupies an area of 148 km^2 in southeastern Arizona. The climate is semi-arid, with an average annual rainfall of 324 mm, lower than in the Yanco region. Most of the rains occur in the form of small scale high-intensity thunderstorms during the summer months as part of the North American Monsoon System (Cosh et al., 2008). Soils are mainly sands and gravel with good drainage. Desert shrubs and short grasses dominate the landscape. The topography is considered as rolling with significant rock cover. Although the climate class of WG is defined semi-arid as the Yanco area, the contrasting landscape properties and precipitation conditions make WG an interesting validation area (Table 1).

It is important to outline that the area extent covered by the networks is different so it may have an impact on the validation process: the MB comprises multiple SMOS pixels through sparse stations and more dense localized sites, the Yanco region covers approximately one SMOS pixel, and the LW and WG cover around 1/4 and 1/16 of the surface of one SMOS pixel. This does not affect the C4DIS processor, which handles input larger surfaces, but it may affect the validation process since the smaller networks may not be representative of the ~40 km surface.

Table 1- Main characteristics of validation areas

	Murrumbidgee	**Yanco**	**LW**	**WG**
Extension	82,000 km^2	3000 km^2	610 km^2	148 km^2
Climate	Semi-arid (west) to humid (east)	Semi-arid	Sub-humid	Semi-arid to arid
Annual precipitation	300 – 1900 mm	400 mm	750 mm	324 mm
Main precipitation periods	Relatively constant at the basin scale	Winter, spring	Autumn, spring	Summer (intense, localized)
Soils	Clayey (west) to sandy (east)	Silty-loam	Sands, loams and clays	Sands and gravel
Topography	Diverse, mountains in the east	Flat	Moderate rolling	Rolling

2.2 SMOS soil moisture data

The SMOS satellite was launched in November 2009. SMOS has global coverage with a revisit period of 3 days at the equator, with ascending (A) overpass at 6:00 am and descending (D) overpass 6:00 pm local solar time. The SMOS instrument is a passive 2D interferometer operating at L band (1.4 GHz) (Kerr et al., 2001, 2010). The spatial resolution ranges from 35 to 55 km, depending on the incident angle. The goal is to retrieve SM (first 5 cm) with a target accuracy of 0.04 m^3/m^3 (Kerr et al., 2012).

The C4DIS processor disaggregates the SM provided by the SMOS Level-3 1-day global SM product (MIR CLF31A/D). In this paper, the version 2.72 (in 220 reprocessing mode RE02) product is used. Level-3 (L3) products are presented in NetCDF format on the EASE (Equal Area Scalable Earth) grid, with a grid spacing of ~25x25 km.

The L3 SM products are directly computed from the SMOS Level-1 products at the CATDS. The core of the algorithm for retrieving SM from brightness temperatures is derived from the L2 retrieval algorithm (Kerr et al., 2012; Wigneron et al., 2007). In both processing chains, SM is derived from the combination of multiangular observations. While the L2 chain considers only the multiangular observations of the same day and orbit (ascending/descending), the L3 chain uses several overpasses (3 at most) over a 7-day window. This results in more coverage and robustness for the L3 products (Al-Yaari et al., 2014). Details on the L3 processing algorithm can be found in the Algorithm Theoretical Baseline Document (Kerr et al., 2013) and in the L3 data product description (Kerr et al., 2014).

2.3 MODIS temperature and vegetation data

The C4DIS processor uses three ancillary products at 1 km resolution. Two of them are derived from MODIS acquisitions: LST and NDVI. These are necessary elements for the SEE calculation inside DISPATCH.

The LST datasets are extracted from version-5 MODIS/Terra LST and emissivity daily L3 global 1-km grid products (MOD11A1) and version-5 MODIS/Aqua LST and emissivity daily L3 global 1-km grid products (MYD11A1). The NDVI dataset is extracted from the version-5 MODIS/Terra vegetation indices 16-day Level-3 global 1-km grid product (MOD13A2).

The MODIS products are retrieved from the NASA Land Processes Distributed Active Archive Center (LP DAAC). They are presented in sinusoidal projection at 1 km resolution (Solano et al., 2010; Wan, 1999, 2006). The disaggregation approach requires the NDVI dataset acquired within the last 15 days and the LST datasets of the day before, the same day and the day after. The MODIS products are available between 1 and 9 days after the acquisition day.

2.4 Digital Elevation Model

The C4DIS processor requires elevation information, which is extracted from the GTOPO30 Digital Elevation Model (DEM) product available in the WGS84 sphere at 30-arc second resolution. The GTOPO30 product is distributed by the U.S. Geological Survey’s EROS Data Center (USGS, https://lta.cr.usgs.gov/GTOPO30).

3. The CATDS Level-4 Disaggregation (C4DIS) processor

The CATDS Level-4 (L4) Disaggregation (C4DIS) processor is the first operational version of the DISPATCH algorithm. The C4DIS processor selects the best algorithm and parameter configuration according to past DISPATCH studies and the latest research (Merlin et al., 2006, 2009, 2010a, 2010c, 2012, 2013). It also makes possible to obtain disaggregated SM on a global and daily basis (under the assumption of no cloud-covered scenes and availability of input data). The C4DIS products have been marked as ‘scientific’ products because the algorithm is still evolving: their access will be granted on demand for specific areas of the world. In this and the following sections, we describe both the DISPATCH prototype and the C4DIS processor.

3.1 DISPATCH algorithm

DISPATCH relies on a SEE term to model the spatial variability over the low-resolution (LR) SMOS pixel. The first step is to account for the SEE term at HR, described as a linear function of soil temperature:

$$\mathrm{SEE}_{\mathrm{HR}} = (\mathrm{T}_{\mathrm{s,max}} - \mathrm{T}_{\mathrm{s,HR}}) / (\mathrm{T}_{\mathrm{s,max}} - \mathrm{T}_{\mathrm{s,min}}) \quad (1)$$

Soil ($\mathrm{T}_{\mathrm{s,HR}}$) and vegetation ($\mathrm{T}_{\mathrm{v,HR}}$) temperatures are derived from LST and NDVI datasets as in Merlin et al., (2012), where the surface temperature is partitioned into its soil and vegetation components according to the trapezoid method of Moran et al. (1994). Soil temperature is calculated as follows:

$$\mathrm{T}_{\mathrm{s,HR}} = (\mathrm{T}_{\mathrm{MODIS}} - \mathrm{f}_{\mathrm{v,HR}}\mathrm{T}_{\mathrm{v,HR}}) / (1-\mathrm{f}_{\mathrm{v,HR}}) \quad (2)$$

with $\mathrm{T}_{\mathrm{MODIS}}$ being the MODIS LST and f_{v} the MODIS-derived fractional vegetation cover. Here, the fractional vegetation cover is calculated as:

$$\mathrm{f}_{\mathrm{v,HR}} = (\mathrm{NDVI}_{\mathrm{MODIS}} - \mathrm{NDVI}_{\mathrm{s}}) / (\mathrm{NDVI}_{\mathrm{v}} - \mathrm{NDVI}_{\mathrm{s}}) \quad (3)$$

with $\mathrm{NDVI}_{\mathrm{MODIS}}$ being the MODIS NDVI, $\mathrm{NDVI}_{\mathrm{s}}$ the NDVI for bare soil (set to 0.15), and $\mathrm{NDVI}_{\mathrm{v}}$ the NDVI for full-cover vegetation (set to 0.90).

The vegetation temperature $T_{v,HR}$ is calculated according to the “hourglass” approach (Moran et al., 1994, Merlin et al., 2012):

$$T_{v,HR} = (T_{v,min} + T_{v,max}) / 2 \quad (4)$$

At this point, vegetation ($T_{v,min}$, $T_{v,max}$) and soil ($T_{s,min}$, $T_{s,max}$) temperature end-members are estimated depending on the amount of vegetation. Given the minimum and maximum LST values of the scene $T_{MODIS,min}$ and $T_{MODIS,max}$, and the f_v values associated to the same pixels, $f_{v,Tmin}$ and $f_{v,Tmax}$, the following approximations hold (Merlin et al., 2013):

I) When the vegetation portion is low at $T_{MODIS,min}$ ($f_{v,Tmin} < 0.5$), then $T_{s,min} = T_{v,min} = T_{MODIS,min}$

II) When the vegetation portion is considerable at $T_{MODIS,min}$ ($f_{v,Tmin} >= 0.5$), then $T_{v,min} = T_{MODIS,min}$ and $T_{s,min}$ is derived from Eq. 2, with $T_v = T_{v,min}$

III) When the vegetation portion is low at $T_{MODIS,max}$ ($f_{v,Tmax} < 0.5$), then $T_{s,max} = T_{MODIS,max}$ and $T_{v,max}$ is derived from Eq. 2, with $T_s = T_{s,max}$

IV) When the vegetation portion is considerable at $T_{MODIS,max}$ ($f_{v,Tmin} >= 0.5$), then $T_{v,max} = T_{MODIS,max}$ and $T_{s,max}$ is derived from Eq. 2, with $T_v = T_{v,max}$

Note that LST has been preliminary corrected for elevation effects (decrease of air temperature with altitude) by using the DEM information at HR (Merlin et al., 2013):

$$T_{MODIS} = T_{MODIS\text{-}ori} + \gamma(H_{HR} – H_{LR}) \quad (5)$$

with T_{MODIS} being the topography-corrected LST used in the previous equations, $T_{MODIS\text{-}ori}$ the original MODIS LST, γ (°C m^{-1}) the mean lapse rate (set to 0.006 °C m^{-1}), H_{HR} the altitude of the MODIS pixel and H_{LR} the mean altitude within the LR pixel.

In a second step, the semi-empirical linear model of Budyko (1956) and Manabe (1969) is used to link the surface SM (0-5 cm) and the SEE terms. According to Merlin et al. (2013), the linear model is a good approximation for kilometer scales so the SEE for each HR pixel can be written as:

$$SEE_{HR} = SM_{HR} / SM_p \quad (6)$$

where SM_p is a parameter estimated at LR at each execution from daily SM and SEE observations as follows:

$$SM_p = SM_{LR} / SEE_{LR} \quad (7)$$

with SM_{LR} the radiometer-sensed SM and SEE_{LR} the average of the SEE_{HR} values inside the LR pixel.

The disaggregation is finished by applying a first order Taylor series to the SM-SEE model at each HR pixel (downscaling relationship). The corresponding disaggregated SM is:

$$SM_{HR} = SM_{LR} + SM'(SEE_{LR}) \times (SEE_{HR} - SEE_{LR}) \quad (8)$$

with $SM'(SEE_{LR})$ the partial derivative of SM relative to SEE at LR (SM_p).

3.2 DISPATCH operational implementation

Following the methodology introduced in Merlin et al. (2012), C4DIS executes DISPATCH on a set of possible combinations of input datasets, producing multiple HR outputs that are averaged together into a single final disaggregated SM field (SM_HR). The rationale behind this is to account for the uncertainty of the approach and to reduce independent random errors (Malbéteau et al., 2016b; Merlin et al., 2012). The input ensemble is formed by 4 downsampled instances of the original L3 SM dataset and up to 6 LST datasets corresponding to 3 consecutive days of MODIS acquisitions (Aqua and Terra overpasses). This means that each SM_HR output comes from the composition of up to 24 DISPATCH outputs (up to 24 input SM-LST possible pairs).

SMOS original datasets are downsampled in order to work at the radiometer resolution. SMOS L3 products are provided on a 25 km grid, which can be up to half of the original SMOS resolution (35-50 km). The four SM datasets are derived from the original SM map by sampling the data at 50 km and are assumed to be independent. This is not totally true, since grid cells depend on the surrounding cells from a radiometric perspective, but helps to potentially reduce (and provide an estimate of) random errors in the SM_HR data. Regarding the selection of 6 MODIS LST datasets from 3 consecutive days, it is assumed that SM fields are spatially stable for periods of at least 1 day around the SMOS overpass time. This 3-day derived product with daily estimated SM_p is referred as the ‘sm1k3d’ product in Malbéteau et al. (2015) and is the one built by the C4DIS processor. The 3-day product has much better temporal coverage than its 1-day counterpart (‘sm1k1d’), but the uncertainty associated to the methodology is expected to be higher since the temporal stability assumption can be often violated by precipitation and irrigation events.

There is no dedicated dataset in the C4DIS product that specifies explicitly whether the 3-days stability condition is respected or not. In the future, this will be achievable with the use of ancillary precipitation information, for example. Meanwhile, in addition to the SM_HR dataset, two more datasets are produced as indicators of the aggregation of the DISPATCH ensemble: the STD dataset, which is the standard deviation of the up to 24 disaggregated SM fields, and the COUNT dataset, which is the size of the ensemble. The aggregation is conducted if at least 3 SM fields are generated, so the COUNT values range from 3 to 24. In this paper, we study the STD and the COUNT datasets as potential sources of information for a future quality control flag (section 5.5).

Finally, the current version of DISPATCH filters out any LST pixel values that have associated QC flags different from 0 and 17, which correspond to maximum LST quality (error <1K) and maximum emissivity error of 0.01 and 0.02 respectively (Solano et al., 2010; Wan, 2006). Areas with more than 1/3 of their surface covered by clouds are also discarded. Differences between the operational and the prototype versions of DISPATCH are summarized in Table 2.

Table 2 - Main differences between the DISPATCH operational implementation in the C4DIS processor and the previous prototype versions

	C4DIS processor	**(Merlin et al., 2013)**	**(Merlin et al., 2012)**
SEE model	Linear (Budyko, 1956; Manabe, 1969)	Linear (Budyko, 1956; Manabe, 1969)	Non-linear (Noilhan & Planton, 1989)
Calculation of T_v	“Hourglass” approach (Moran et al., 1994)	“Hourglass” approach (Moran et al., 1994)	“Hourglass” approach (Moran et al., 1994)
Calculation of temperature end-members ($T_{s,min}$, $T_{s,max}$, $T_{v,min}$, $T_{v,max}$)	Estimated by a simpler approach based on the combination of LST and f_v	Estimated by a simpler approach based on the combination of LST and f_v	Estimated by plotting MODIS LST against MODIS albedo and NDVI within the LR pixel (Merlin et al., 2010b)
Input SM data	SMOS L3 SM	SMOS L2 SM	SMOS L2 SM

Input LST data	“sm1k3d” mode (3x2 input LST datasets)	“sm1k1d” mode (1x2 input LST datasets)	“sm1k3d” mode (3x2 input LST datasets)
Input DEM data	GTOPO30	GTOPO30	Not implemented
LST filtering	Yes, QC flags 0 and 17	Yes, QC flags 0 and 17	No
Cloud-free threshold	0.67	0.90	0.90
Sea-free threshold	0.90	0.90	Not implemented

3.3 Pre-processor

The C4DIS pre-processor prepares the input ensemble that is required by DISPATCH. The pre-processor uses the MODIS sinusoidal tiling system as the execution reference, meaning that the processor is executed for the SMOS and ancillary data contained within each MODIS tile bounds. More information about the grid can be found in http://modis-land.gsfc.nasa.gov/MODLAND_grid.html. The SMOS and ancillary data inside the tile bounds are selected and re-projected to an equal-spaced lat-lon WGS84 grid. Considering that ancillary products are presented in different datums and grids, the choice of the WGS84 projection minimizes the total number of resampling operations.

The pre-processor is divided into modules for file format transformation, dataset extraction, re-projection and re-gridding. As explained in the previous section, DISPATCH requires 4 subsampled instances of SMOS data and up to 6 LST datasets. As a consequence, the re-projection and re-gridding are sensible operations that deserve being explained in detail.

The pre-processor outputs are re-projected to the same WGS84 projection, but resampled to different resolutions: SMOS subsampled rasters are provided on 0.4° grids while ancillary raster data are provided on a 0.01° grid. The SMOS 0.4° grids are derived from an original global grid at 0.2° by sliding a 0.4° window over it, so that the pixel centers are coincident. Based on this, the SM values become representative of the double of the original grid resolution 0.2°, which approximately matches the average SMOS resolution. The disaggregation is only performed in the intersection area between the 4 SMOS grids and the ancillary data grid (Figure 1).

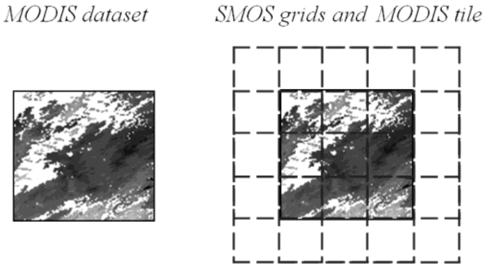

Figure 1 – Simplistic representation of the relation between the SMOS subsampled grids (at 0.4°) and the re-projected ancillary data at 0.01°. The extent of the re-projected ancillary image (LST, NDVI, etc.) matches the intersection of the four SMOS grids. The disaggregation is only applied in this overlapping zone.

3.4 Post-processor

The C4DIS post-processor transforms the DISPATCH outputs into the CATDS format. It includes two significant transformations that impact the disaggregated data. First, in the case that DISPATCH generates negative SM values (which is mathematically possible), the post-processor clips them to 0 to respect physical meaning. Second, since the outputs of DISPATCH are presented in local time and day, the post-processor assigns to them the corresponding UTC time and day to keep consistency with other SMOS products.

3.5 Assumptions and applicability domains of the algorithm

The application requirements of the C4DIS processor are directly inherited from DISPATCH. The following considerations must be taken into account:

- *Cloud free conditions*: soil temperature can only been retrieved from optical sensors if clouds are not present. C4DIS products show data gaps associated with clouds.
- *Low vegetation cover*: The LST-NDVI trapezoid describes a zone of values where no useful disaggregated data can be produced since LST is mainly controlled by vegetation transpiration, with no sensitivity to surface SM (Merlin et al., 2013). Sites with partial fractional vegetation cover at the 1 km resolution are desired.

- *Moisture-driven evapotranspiration*: the disaggregation relies on the dependence established between LST, evapotranspiration and SM. Some climates exhibit low dependency between those variables. Typically, climates characterized as energy-limited, like humid climates, exhibit a weaker moisture-evaporation coupling.

- *Medium to high spatial variability*: the MODIS-derived SEE is computed with a polygon method that relies on LST and reflectance end-members (Moran et al., 1994). In the current version, DISPATCH is contextual and thus heterogeneous scenes with meaningful dry-wet contrast are needed in order to ensure good end-members accuracy (Merlin et al., 2010a). Note that LST end-members could be estimated using available meteorological data (Moran et al. 1994) independently from the surface (wet/dry) conditions observed at the 1 km resolution within the LR pixel (Stefan et al., 2015).

- *Accuracy of the SM_p parameter*: the SM_p parameter is calculated at LR scale by using a linear relationship that has been studied as suitable for kilometer scales (Merlin et al., 2013). It is based on the assumption that the sub-pixel variability of SM_p at HR is negligible. Soil characteristics (texture, porosity, etc.) may impact the relationship between SEE and SM and thus SM_p. Hence, the current versions of C4DIS and DISPATCH should perform better in areas with homogeneous soil characteristics where the intra-pixel spatial SM variability is mainly due to forcing agents, namely precipitation and irrigation.

- *Mismatch of overpass times*: the C4DIS processor uses MODIS LST datasets at 6 different timestamps. This is based on the assumption that the SM pattern is maintained over a period of 3 days, with no rain events occurring in between.

- *Mismatch of sensing depths*: SMOS L-band SM estimations are representative of the soil first 5 cm content, while MODIS temperature acquisitions are representative of the soil skin layer. DISPATCH assumes that the soil skin temperature is correlated with the soil evaporation process occurring in the 0-5 cm of soil (Merlin et al., 2010a).

3.6 Global product description

- *Coverage, grid and resolution.* C4DIS products are presented in a regular lat-lon grid at 0.01° resolution. The projection is divided in a tiled grid that follows the MODIS sinusoidal tiling system, meaning that the C4DIS tiles are centered at MODIS tiles and follow the same name convention in (h,v) coordinates. Due to reprojection, the tiles present different size. C4DIS products can be generated for all emerged lands (tiles with more than 50 % of land), but since they are tagged as 'scientific' products, the tiles of interest have to be delivered on demand. For this study, the following tiles have been produced: (29,12) and (30,12) for the validation over the MB, (09,05) for LW and (08,05) for WG. Figure 2 shows annual averages of C4DIS products for the selected tiles. The extension and border of the tiles are easily distinguishable.

- *Availability and timeliness.* The delivering of C4DIS products is determined by the availability and timeliness of the input datasets. The limiting dataset is the MODIS MOD13A2 product (NDVI), which is valid for a period of 15 days starting at its date of acquisition (DoA) but can be delivered some days later. In consequence, C4DIS products for dates DoA to DoA+15 are produced at date DoA+25. In other words, each 16 days the C4DIS products for acquisition dates between 25 to 10 days before are delivered.

- *Datasets and quality control.* We cannot provide a full-proof quality flag given the current status of the processor and the algorithm. Nevertheless, the output COUNT and STD datasets can help to assess the quality of the SM_HR dataset. Combining these datasets with additional ancillary data like precipitation or MODIS/SMOS quality flags, may help to build a quality control dataset in the future.

As introduced in Section 3.2, the COUNT field determines the number of SM-LST combinations used by DISPATCH to produce one output. Low COUNT values indicate missing input data as result of diverse reasons: SMOS RFI contamination, MODIS cloudy scenes, failures in the SMOS/MODIS acquisitions delivering, etc. SM_HR fields generated when low COUNT values are present do not profit from the reduction in independent random errors as result of averaging. The STD field contains the per-pixel standard deviation of the up to 24 disaggregated datasets with respect to the averaged output SM_HR.

Low values of STD are desirable since they reveal temporal persistency of both temperature and moisture variables. High values may indicate external forcing agents (precipitation and irrigation) within the 3-days window.

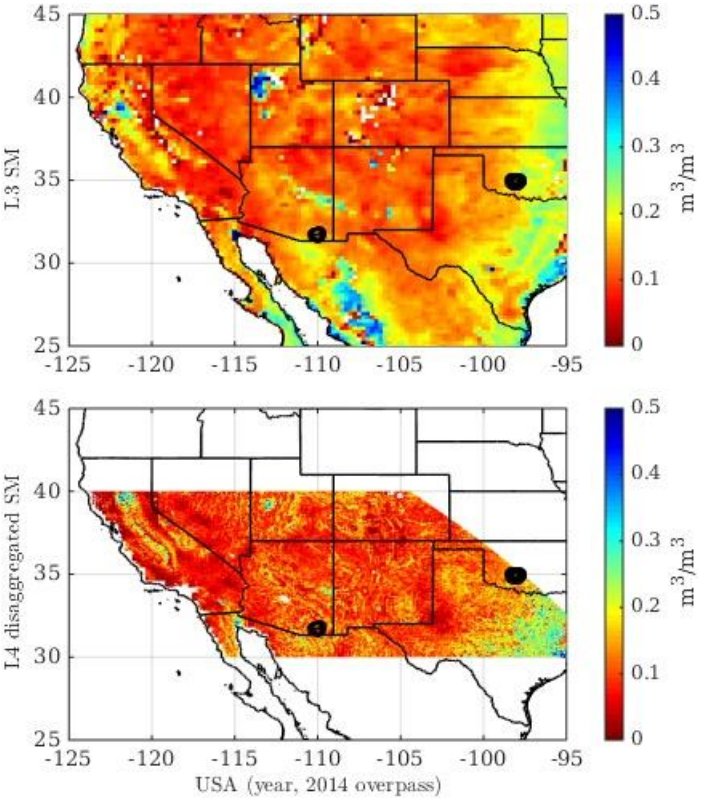

Figure 2 - Year averages of SMOS L3 and L4 disaggregated products (ascending orbit) for part of the USA and for the year 2014. The L4 figure includes only the tiles (08,05) and (09,05), joined together. The black circles correspond, from left to right, to the location of Walnut Gulch and Little Washita validation networks.

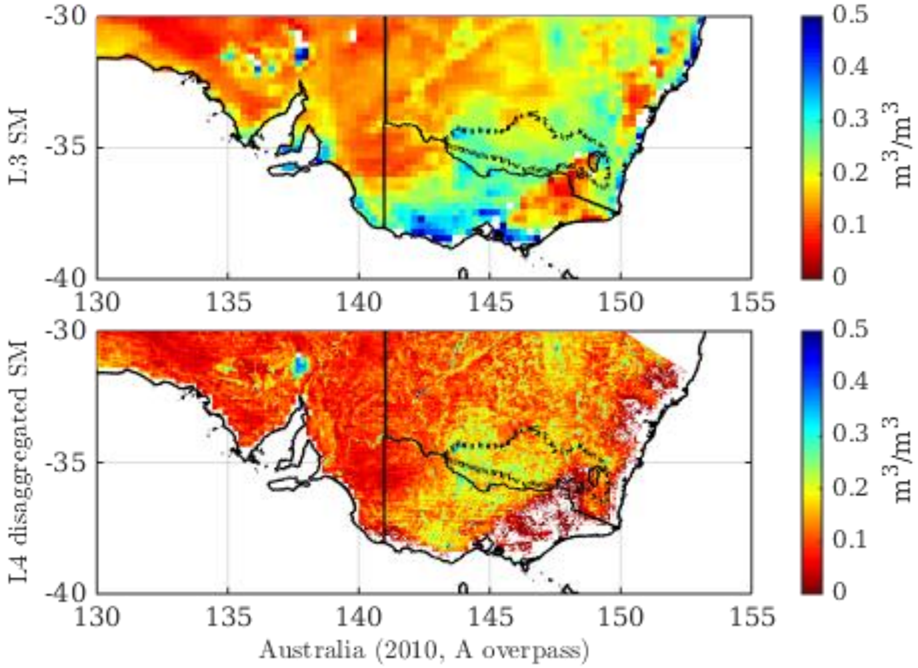

Figure 3 - Year averages of SMOS L3 and L4 disaggregated products (ascending orbit) for part of Australia and for the year 2010. The L4 figure includes part of the tiles (29, 12) and (30,12), joined together. The dotted line depicts the boundary of the Murrumbidgee catchment.

4. Analysis Methodology

Our analysis involves two main approaches: qualitative assessment of disaggregated SM maps and statistical evaluation. The statistical evaluation consists on comparing the L3 SMOS product (LR) and the L4 product (HR) against the *in situ* SM by using standard statistical metrics (e.g. correlation, bias, etc.). This can be accomplished in the spatial or in the time domain. We base the statistical evaluation on the assumption that the 1 km pixel is more representative of the *in situ* measurement than the whole LR pixel.

In order to assess the relative spatial performance of both L3 and L4 products at HR, we directly compare the station measurements to the satellite retrievals, without aggregating them at LR. In the subsequent sections, MB refers to the whole Murrumbidgee network, including Yanco area. Yanco only refers to the 12 stations contained in this region.

4.1 Data preparation

We filter L3 and L4 SM time series for radio frequency interference (RFI) by removing pixels having more than 10 % RFI probability. The RFI information is extracted from the same CLF31A/D product and accounts for the percentage of brightness temperatures acquisitions affected by RFI presence (Kerr et al., 2013; Oliva et al., 2012). In addition, regarding the *in situ* data, we only keep the SM values at the SMOS overpass times. Finally, we filter the three SM time series (in situ, L3 and L4) for common dates with valid SM values (>0.0 m^3/m^3).

4.2 Analysis of the temporal and spatial variability of the *in situ* SM

As expected for any data disaggregation approach, the application of DISPATCH is relevant when the SM spatial variability at the downscaled resolution is larger than the output uncertainty. Since the current version of DISPATCH relies on the spatial contrast of LST and SM of the scene, a preliminary study on the spatial SM variability of the validation areas is desired. In homogeneous SM landscapes, the output uncertainty is likely to be greater than the spatial gain provided at HR by disaggregation.

Similarly, it is desirable that the evaluation include *in situ* time series spanning the full range of SM conditions and seasonal changes. In other words, the temporal standard deviation (σ) should be large enough so that all the states of the SM variable are represented and no selection bias is present. Additionally, stations exhibiting very different temporal σ may suggest landscape spatial heterogeneity: soil characteristics like texture, vegetation and topography affect the dry-down process, generating different extreme values in time.

Based upon the considerations discussed above, the evaluation of the performance of the C4DIS products should include a preliminary assessment of the spatial and temporal SM variability of the validation networks. The performance of DISPATCH outputs over MB and Yanco has been identified as rather satisfactory in recent studies (Malbéteau et al., 2016b; Merlin et al., 2012), which makes them good references for spatial and temporal σ.

4.3 Classical metrics

Given the spatial mismatch between *in situ* and satellite estimations and the spatial scarcity of ground stations, most classical satellite validation campaigns only evaluate the temporal dimension, by means of metrics like correlation (R), root mean square error (RMSE) and bias (B) (Albergel et al., 2012; Albergel, et al., 2013; Entekhabi, et al., 2010b; Bitar et al., 2012). In this study, we use similar temporal analysis but we also include an evaluation in the spatial domain since disaggregation techniques aim at producing better spatial representation. The spatial statistical analysis consists of computing the metrics between the satellite and *in situ* values for each day, then, deriving the average of each metric for the whole period. We deliberately establish a minimum of 5 points per day to compute the metrics.

Herein, instead of the RMSE, we use as error metric the standard deviation of the error (Eq. 9) (Mood et al., 1974; Salkind, 2010), which is a non-biased estimation of the error and so it is not compromised by the bias in the mean and amplitude of the time series that affects the RMSE. The relationship between both metrics is written in Eq. 10 and 11. Since we already use multiple terms to refer to different standard deviation measures and datasets in this paper (σ, STD), we will refer to this metric as unbiased-RMSE or ubRMSE (Entekhabi et al., 2010b). Given that the 1 km pixels are in general heterogeneous and that the ground data also present measurement uncertainties, the term ‘error’ has been replaced by ‘difference’ in these metrics, i.e. RMSD and ubRMSD.

$$\mathrm{ubRMSD} = \sqrt{} \, E\{\, [(SM_{satellite} – E\{SM_{satellite}\}) – (SM_{insitu} – E\{\, SM_{insitu}\, \})]^2\} \quad (9)$$

$$\mathrm{RMSD} = \sqrt{} \, E\{(SM_{satellite} - SM_{insitu})^2\} \quad (10)$$

$$\mathrm{ubRMSD} = \sqrt{} \, (\mathrm{RMSD}^2 - B^2) \quad (11)$$

where E{·} is the expectation operator, $SM_{satellite}$ and SM_{insitu} the satellite and the *in situ* SM time series.

We include one additional metric to assess the efficiency gained in spatial representativeness: the slope (S) of the regression line between *in situ* and satellite estimates:

$$S = R \cdot \sigma_{satellite} / \sigma_{insitu} \quad (12)$$

with $\sigma_{satellite}$ and σ_{insitu} being the standard deviations of satellite and *in situ* SM, respectively. The S metric can help to understand how much better the SM redistribution is represented after the disaggregation process. Whereas aggregation systematically decreases the $\sigma_{satellite}$, disaggregation specifically aims to improve the spatial representation of satellite SM by increasing the $\sigma_{satellite}$ at the level of σ_{insitu}, while keeping a significant R. Mathematically speaking, R is the slope of the standardized regression line, and S is scaled by the σ values of both data ensembles (Rodgers & Nicewander, 1988). Since the σ_{insitu} is fixed, S is more sensitive than R to changes in $\sigma_{satellite}$. In summary, an increase in random uncertainties (larger ubRMSD, smaller R) in disaggregated SM might be acceptable if S is closer to 1. Note that the random uncertainties in satellite SM can be significantly reduced via the techniques of data assimilation in land surface models, but the systematic errors associated with the mismatch between data resolution and model application scale are more difficult to take into account at HR (Merlin et al., 2006).

Finally, the metrics here (S, R, ubRMSD, B) assume that a linear relationship exists between the two datasets compared. This means that they cannot replace the visual assessment of the data. In the general case, both SMOS L3 and disaggregated SM may exhibit non-linear behavior with respect to *in situ* SM.

4.4 Relative performance metrics

Comparing the improvement/degradation in statistics for different cases of study (networks, filtering, time period, etc.) may be difficult: we propose as solution to calculate their relative gains as introduced in Merlin et al. (2015). Briefly, the gain is a measure of the improvement in the statistics obtained for the L4-*in situ* pair with respect to the L3-*in situ* pair. The gain can range from -1 to 1, where positive values indicate disaggregated data having better correspondence with *in situ* than LR data. In this study, we keep the nomenclature of Merlin et al. (2015) and we add a new gain term for the ubRMSD (see Table 3). The gains are calculated as in Eq. 13 for in S and R metrics, and as in Eq. 14 for B and ubRMSD.

$$G_X = -\,(|1-X_{L4}|-|1-X_{L3}|)\ /\ (|1-X_{L4}|+|1-X_{L3}|) \quad (13)$$

$$G_X = -\,(|X_{L4}|-|X_{L3}|)\ /\ (|X_{L4}|+|X_{L3}|) \quad (14)$$

where X designates the metric (S, R, B, ubRMSD), X_{L4} the value of the metric when disaggregated SM is compared against *in situ*, and X_{L3} the value of the metric when L3 SM is compared against *in situ.*

Table 3 - List of performance metrics used in this study, from (Merlin et al., 2015)

Gain(S) …….........	G_{EFFI}
Gain(R) …….........	G_{ACCU}
Gain(B) …….........	G_{ROBU}
Gain(ubRMSD)	G_{ubRMSD}

5. Results and discussion

This study seeks to provide a first assessment on the applicability of the DISPATCH-based processor under different climatic and landscape conditions. It also attempts to provide statistical guidelines on the *a priori* suitability of a geographical area for the production of meaningful C4DIS fields. The analyses span the 01/06/2010 to 31/12/2014 period for the MB network and Yanco area and the 01/06/2010 to 31/12/2014 period for the LW and WG networks. The SMOS data collected during the commissioning phase (until 31/05/2010) is discarded.

5.1 Preliminary analysis

In order to predict the performance of the processor, we conduct a statistical analysis on the in situ SM data. We derive conclusions about their temporal and spatial variabilities by looking at their distribution of SM values and their distribution of 'spatial σ' and 'temporal σ'. The 'spatial σ' (upper row in Figure 4) is the standard deviation of the SM distribution on each day. The 'temporal σ' (middle row) is the standard deviation of the SM series of each station.

As stated in section 4.2, we consider the in situ SM distribution characteristics of MB and Yanco networks as reference in the present study. The spatial σ plot shows narrower distributions for LW and WG, and the mean value is much lower for the latter (0.03 m^3/m^3). This means that the spatial variability at LW and WG seen at the satellite overpass times is lower than in the reference cases, so we expect poorer performances in the spatial domain.

In the temporal domain (middle row of Figure 4), the mean variability of LW and WG networks is lower than that of the Australian cases. The SM distribution of WG (4th column) shows a very strong peak near zero that accounts for almost the half of the samples. Under these conditions, we expect WG to be the network with worst temporal performance of C4DIS products, while LW should behave similarly to MB and Yanco. It is important to mention that LW and WG only represent a portion of a SMOS pixel and the *in situ* samples only concern some HR pixels in space, so the distributions depicted here serve only as approximation.

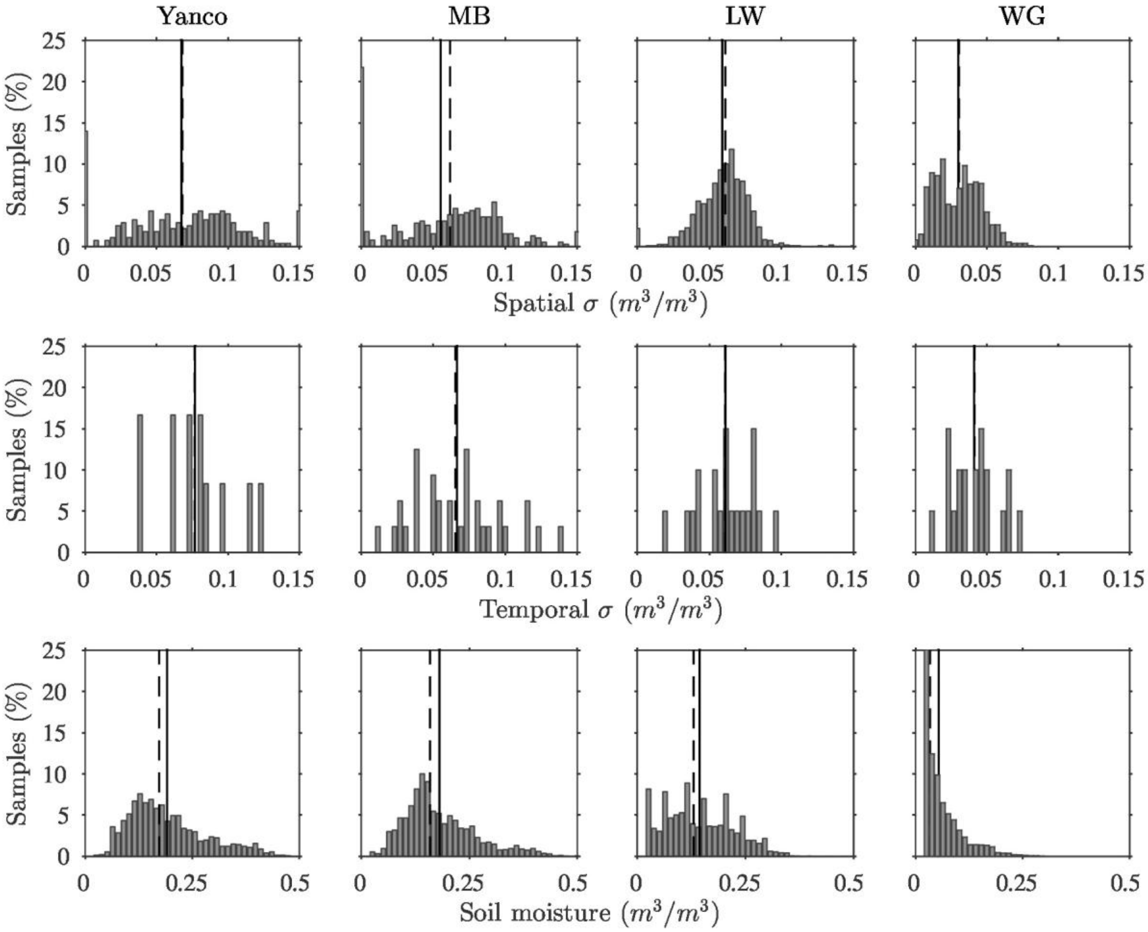

Figure 4- Distribution of spatial and temporal standard deviations and SM values for the in situ samples of Yanco, MB, LW and WG (1st to 4th columns respectively) at the SMOS overpass times. Number of bins of the histograms is 40. The median of the distributions is depicted in dashed line and the mean in solid line. The WG soil moisture maximum percentage is not shown (right-down graph) for readability and it reaches 47 % of the samples.

5.2 Qualitative examples

The qualitative inspection of disaggregated SM maps for MB, Yanco, LW and WG, shows that the L4 product is able to reveal spatial entities like small and sparse water bodies.

Figures 5 and 6 contain sample outputs of the C4DIS processor on cloud-free days for the four areas. In the MB picture (Figure 5), the Murrumbidgee river is revealed thanks to disaggregation, while the south-eastern region is empty due to clouds and the SMOS non-retrieved pixels over the mountains. In Figure 6, disaggregation does not help reveal the Little Washita river course but it does with the surrounding lakes.

The processor fails to display any spatial pattern inside the WG watershed. These maps are in agreement with the evaluation in the previous section.

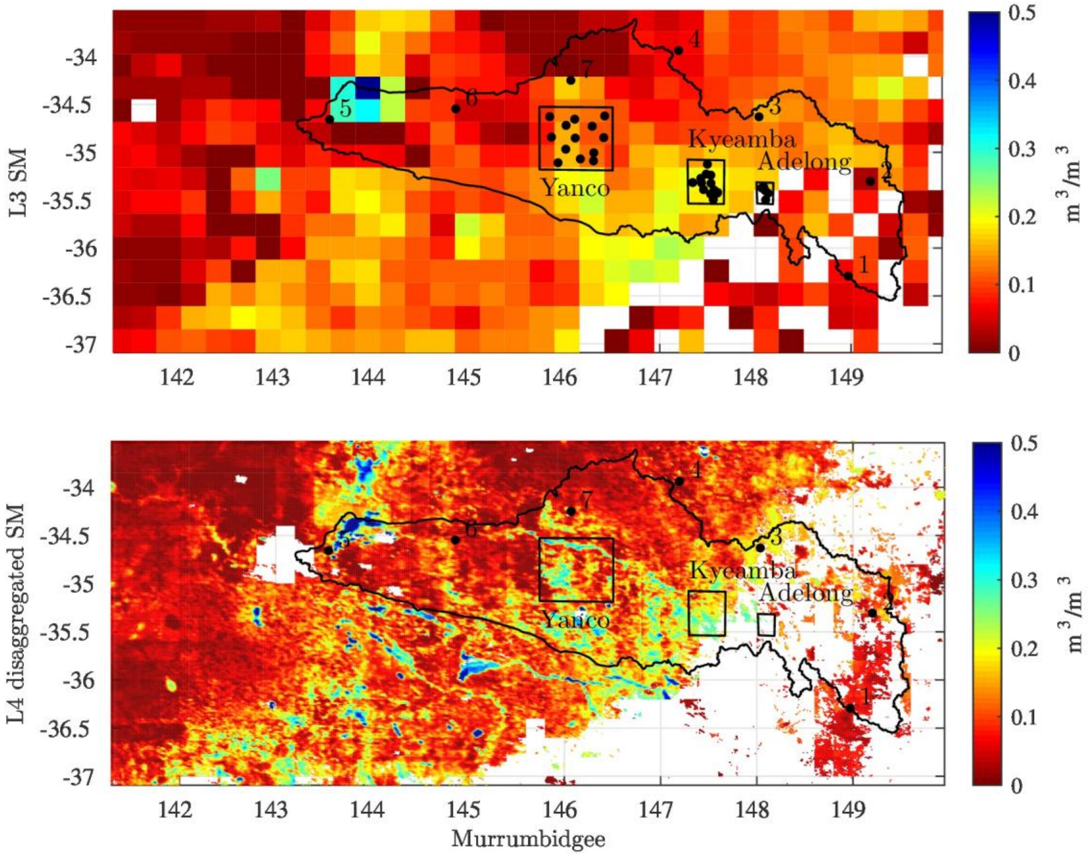

Figure 5 - Maps of L3 SM (CLF31D) and L4 disaggregated SM for MB watershed on 22/11/2010 for the SMOS descending overpass.

Yanco maps are a good example of the usefulness and relevance of the C4DIS products when the algorithm assumptions are met. Figure 7 shows the Yanco area with the limits of the Coleambally Irrigation Area (CIA) units superimposed. At a first glance, the L4 SM map reveals the farms that are actually irrigated, while original SM map do not.

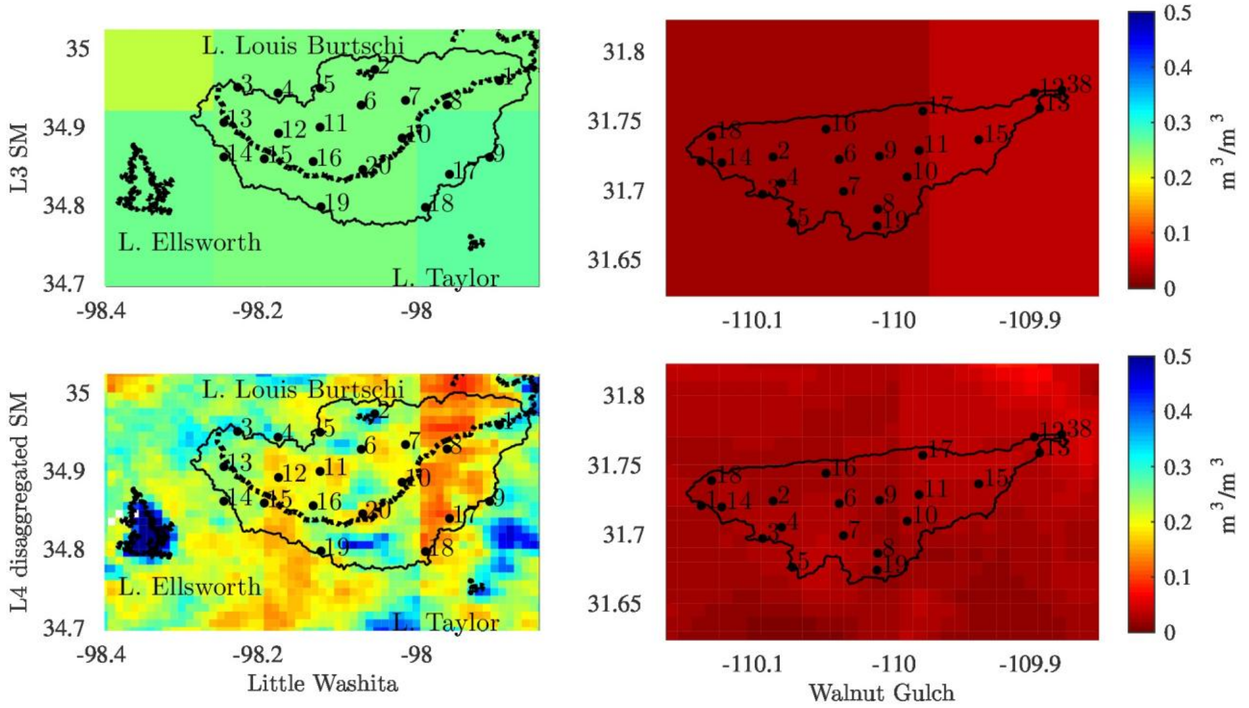

Figure 6 – Maps of L3 SM (CLF31A) and L4 disaggregated SM for LW (left column) and WG (right column) watersheds on 02/05/2011 and 01/05/2011 respectively. Solid black contours correspond to watershed boundaries. In the left column, the bold dotted line in the middle of the watershed correspond to the Little Washita river and the bold dotted contours to surrounding lakes.

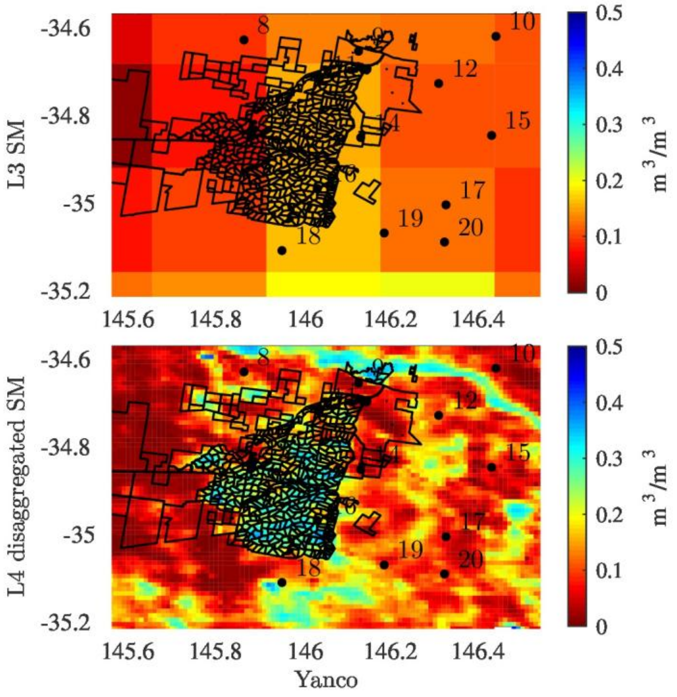

Figure 7- Maps of L3 SM (CLF31D) and L4 disaggregated SM for Yanco area on 22/11/2010. Black lines represent the contours of Coleambally irrigated farms.

Finally, we show in Figure 8 a series of C4DIS disaggregated outputs between the 4th and the 18th day of 2011. We can identify in detail the areas affected by the floods that touched the states of New South Wales and Victoria on those days. Likewise, we see how the dry-down process is faster in some small areas than in others (west of Yanco).

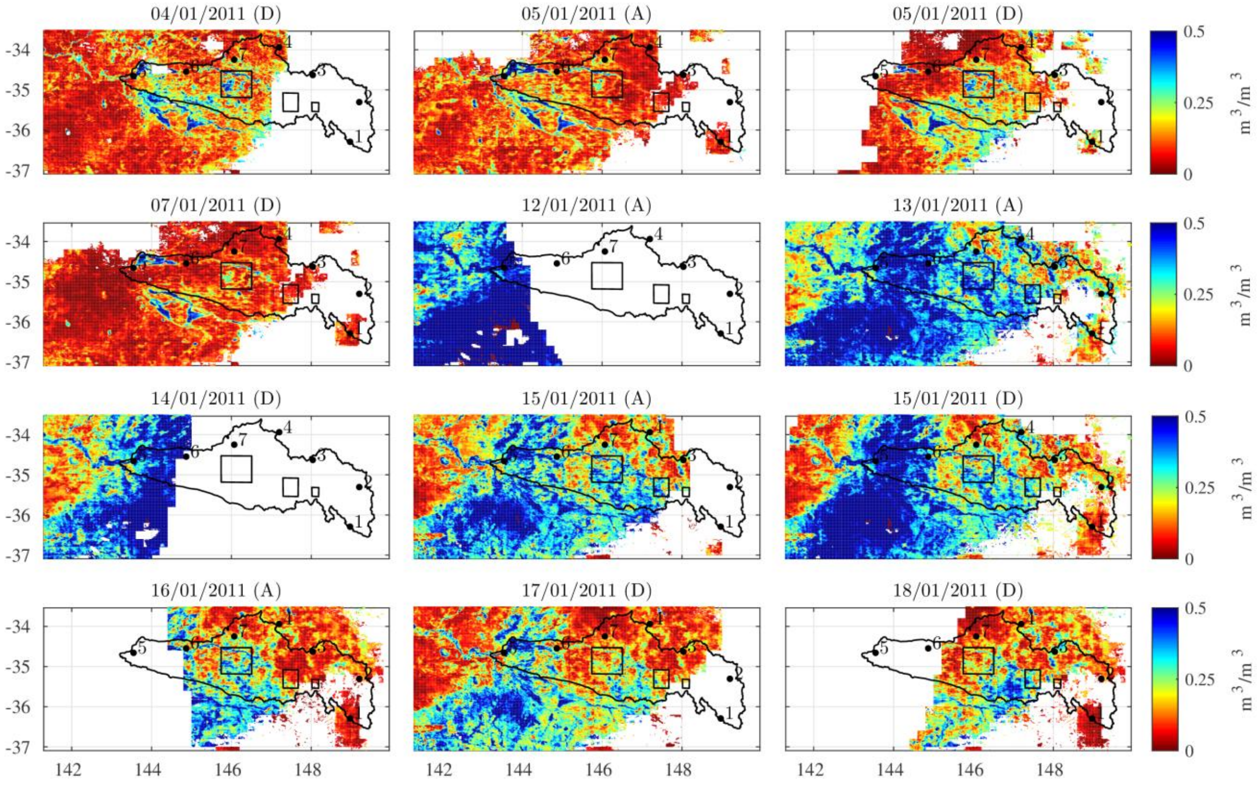

Figure 8 - Maps of L4 disaggregated SM for MB on the first days of January 2011, showing the progression of floods that affected New South Wales and Victoria states. The title of each image contains the date and the SMOS overpass ('A' for ascending, 'D' for descending).

5.3 Spatial evaluation

In this section, the L4 and L3 SM products are compared at HR on a daily basis against the *in situ* measurements.

Table 4 shows daily statistics averaged over the periods of analysis. When comparing the statistics obtained for L3 and L4 products in MB and Yanco networks, it is noted an important enhancement of the S and the R values, ranging between 0.24-0.32 and 0.09-0.17, respectively. Results are consistent with the conditions of the area, especially those of Yanco (semi-arid climate with SM spatial heterogeneity dominated by irrigation). Spatial B is maintained while ubRMSD increases (around 0.02 m^3/m^3) which can be explained by the added uncertainty when combining data from different sources.

LW and WG statistics are much poorer than MB ones: R and S never exceed 0.11. The reasons for that can be found in both the algorithm and the conditions of the validation area. First, the L3 statistics (R and S) are much worse in the American than in the Australian networks, which may entail uncertainty present in the LR product that is propagated to the L4 product. Second, according to the preliminary statistical analysis (section 5.1), the spatial σ distribution of WG is narrower and span over lower values than those of the Australian networks. The spatial variability cannot explain however the poor statistics of LW, since here the mean spatial σ is similar to the Australian ones (0.07 m^3/m^3 for Yanco, 0.06 m^3/m^3 for MB and LW). Another important aspect to take into consideration is the mismatch between the validation extent and the SMOS resolution. LW and WG cover only part of the surface of one SMOS pixel (~1/4 and ~1/12 of its equivalent surface, respectively), so the distribution of spatial σ may not be representative of the surface perceived by DISPATCH. All this suggests that a qualitative analysis of the area is strongly recommended.

The LW watershed has rolling relief and a variety of soil textures and vegetation types, which are not considered in the soil temperature equations of DISPATCH. Moreover, its extension is around 4 times smaller than the Yanco area: we can think that a higher heterogeneity within the 1 km pixel would hamper R and S statistics as well. Most importantly, LW climate is defined as sub-humid, so we can expect the link moisture-evaporation to be weak. Concerning WG, the soils are of fast infiltration (sands and gravels), which reduces the apparent SM spatial contrast at the satellite overpass times, a necessary condition for an accurate computation of the DISPATCH SMp parameter.

The comparison of the results here with previous versions of the algorithm can shed light on the pertinence of the choices made in the algorithm since Merlin et al., 2012. Regarding the most recent study, similar spatial statistics for MB and Yanco can be found in Malbéteau et al., 2015, which proves that the performance of the processor is coherent with that of the prototype algorithm. The remaining differences are originated by two factors. First, in our aim to assess the qualities of the entire C4DIS processor, we use as LR SM reference the original SMOS CLF31A/D product, while Malbéteau et al., 2015 employed a reprojected form of the same product used by DISPATCH, which was a reasonable choice from the algorithm point of view. Second, the C4DIS post-processor clips to zero the negative values produced by DISPATCH, a module that was not still implemented at the time of Malbéteau et al., 2015.

Another two former validation campaigns of DISPATCH showed better correspondence with *in situ* measurements, but they were accomplished for specific areas with known high-evaporative demand and for no more than a dozen of dates. For the Murrumbidgee catchment and AACES-I campaign (Merlin et al., 2012), and the Catalunya campaign (Merlin et al., 2013), summer 2010 and 2011 respectively, the correlation values were close to the double of those obtained for MB in this study. However, the AACES-based study also reported negative values for those dates with very dry homogeneous SM scenes. This confirms our hypothesis for WG, were the large number of 'flat' SM scenes is probably behind the unsatisfactory statistics. In the same article of 2012, the AACES-II results (winter), allowed to presum that the weak evaporation-SM coupling was behind negative R values. Our statistics for LW seem to confirm this point, but since the mean R is higher, it suggests that the algorithm might be useful for some periods of the year.

Table 4 - Spatial statistics of Yanco and MB for the period 01/06/2010 to 31/05/2011 and of LW and WG for the period 01/06/2010 to 31/12/2014. 'L3' refers to the comparison between L3 SM and in situ SM and 'L4' refers to the comparison of L4 disaggregated SM and in situ SM. 'A' stands for ascending orbit and 'D' for descending orbit. All the values are expressed in m^3/m^3, except for R and Number of days, which are unitless.

		Yanco		**MB**		**LW**		**WG**	
		L3	**L4**	**L3**	**L4**	**L3**	**L4**	**L3**	**L4**
S	**A**	0.064	0.309	0.086	0.403	0.003	0.047	0.004	0.110
	D	0.080	0.378	0.195	0.430	0.031	0.046	0.017	0.111
R	**A**	0.201	0.316	0.156	0.288	0.030	0.064	0.015	0.102
	D	0.194	0.363	0.251	0.335	0.115	0.057	0.042	0.111
B	**A**	0.018	0.021	0.031	0.035	0.023	0.016	0.031	0.026
	D	0.006	0.011	0.016	0.020	0.023	0.012	0.029	0.026
ubRMSD	**A**	0.072	0.094	0.082	0.103	0.063	0.076	0.030	0.037
	D	0.077	0.091	0.080	0.100	0.062	0.076	0.033	0.040
Nb days	**A**	74		100		573		552	
	D	66		95		557		545	

5.4 Temporal evaluation

For the temporal analysis, we consider the same period and datasets as in section 5.3. We compute statistics on the concatenation of all the SM series within a network. Table 5 displays temporal statistics for the four validation networks. Regarding Yanco and MB, the S metric is better for the HR SM product (between 0.12 and 0.18 higher), which is consistent with the spatial evaluation results. R is slightly degraded in Yanco while maintained in MB. This, and the increase in ubRMSD, can be explained by the temporal uncertainty induced by the processor when considering as inputs observations acquired in different days and times. These results are consistent with previous validation studies of DISPATCH: Merlin et al., 2013 showed that the temporal S could increase between 0.15 to 0.25 after disaggregation, while R being maintained or increased and ubRMSE increased.

In the case of LW , the disaggregated SM (L4) has a slightly better S when compared to *in situ* SM than does L3 SM for both orbits (improvement of +0.06 for A orbit and of +0.03 for D orbit). The same evaluation holds for WG (improvement of +0.05 and of +0.08 for A and D orbits respectively). Like in the Yanco case, disaggregation slightly degrades R and ubRMSD for both SMOS orbits, showing again the increase of random uncertainties attributed to the models and data used by DISPATCH.

Table 5 - Temporal statistics of Yanco and for the period 01/06/2010 to 31/05/2011, and of LW and WG for the period 01/ 06/2010 to 31/12/2014. 'L3' refers to the comparison between L3 SM and in situ SM and 'L4' refers to the comparison of L4 disaggregated SM and in situ SM. In the second column, 'A' stands for ascending orbit and 'D' for descending orbit. All the values are expressed in m^3/m^3*, except for R and Number of points, which are unitless, and RFI percentage, which is in %.*

		Yanco		**MB**		**LW**		**WG**	
		L3	**L4**	**L3**	**L4**	**L3**	**L4**	**L3**	**L4**
S	**A**	0.368	0.489	0.363	0.538	0.406	0.463	0.490	0.544
	D	0.333	0.465	0.383	0.542	0.415	0.441	0.381	0.458
R	**A**	0.432	0.370	0.321	0.377	0.468	0.434	0.468	0.436
	D	0.369	0.356	0.361	0.368	0.460	0.410	0.352	0.366
B	**A**	0.019	0.023	0.033	0.027	0.023	0.017	0.031	0.026
	D	0.004	0.014	0.020	0.019	0.025	0.014	0.030	0.026
ubRMSD	**A**	0.090	0.120	0.105	0.118	0.078	0.088	0.044	0.051
	D	0.095	0.118	0.095	0.118	0.077	0.088	0.052	0.056
RFI perc.	**A**	0.000	-	0.248	-	1.893	-	1.958	-
	D	0.000	-	0.000	-	1.893	-	1.562	-

Nb points	**A**	754	754	1429	9027
	D	723	723	1409	9337

According to our preliminary analysis on in situ temporal σ and SM samples, WG should at least behave differently with respect to the other networks (much narrower distribution of SM values, skewed to the dry section of the range and lower σ variability). However, no significant differences are found in the temporal statistics.

Differences can be appreciated more easily through qualitative inspection of scatter plots (Figure 9). In Yanco and MB plots, the increase in ubRMSD is observed in the more dispersed cloud of points, although the distribution appears slightly closer and more symmetric around the 1:1 line. In the case of LW, we can see that for drier SM conditions (< 0.15 m^3/m^3), disaggregated values are closer to *in situ* values and become equally distributed around the 1:1 line. Since LW climate is sub-humid, evapotranspiration processes are mainly energy-driven; however, we can expect them to be moisture-driven during periods with lower water availability and higher temperatures like summer. This is confirmed in Figure 10, which shows the scatter plot for LW summers. Regarding WG, the scatter plots show no major differences between L3 and L4 data. This is consistent with the very low spatial and temporal *in situ* σ: DISPATCH is operating at the limit of its nominal range at 1 km resolution and the amount of information obtained is not more important than the uncertainty introduced. It outlines also the importance of qualitative assessments: although LW and WG show similar global spatial and temporal statistics, C4DIS disaggregated fields, which are not of interest in WG, are valuable in the case of LW summers.

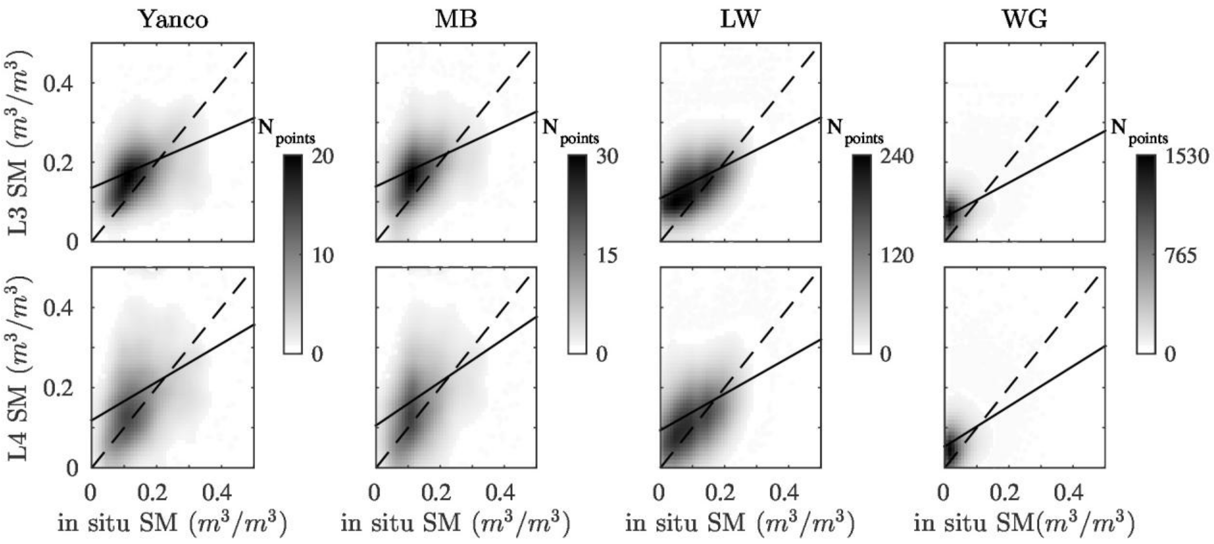

Figure 9 - Scatterplots of original L3 SM (1st row) and L4 disaggregated SM (2nd row) versus in situ measurements for both A and D orbits. The samples here correspond to the periods 06/2010 to 05/2011 for MB and Yanco, and 06/2010 to 12/2014 for LW and WG. Dashed line represents the 1:1 slope and the solid line corresponds to the linear regression line (S statistic).

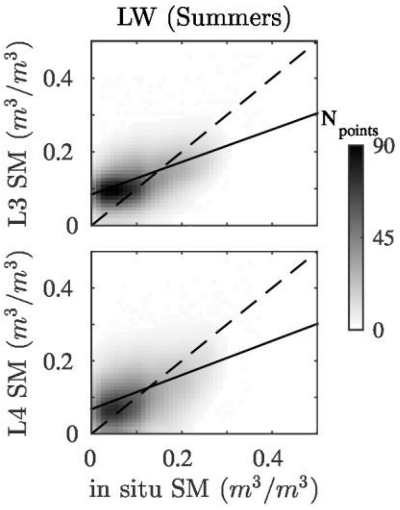

Figure 10 - Scatterplot of L3 SM (1st row) and L4 disaggregated SM (2nd row) against in situ SM samples for LW network for summer periods (June, July and August months of years 2010 to 2014). Dashed line represents the 1:1 slope and the solid line corresponds to the linear regression line (S statistic).

5.5 Analysis of the STD and COUNT datasets

As introduced in section 3.6, the STD and COUNT datasets can help derive conclusions on the quality of the SM_HR values. In this section, we evaluate spatial and temporal statistics on SM samples with different corresponding STD and COUNT values. We first select the samples with values falling inside a given STD or COUNT range of values; then, we compute statistics on the *in situ*, L3 and L4 values for those samples. This analysis is conducted on MB and Yanco networks as USDA networks still show low statistics after filtering for STD and COUNT values. Herein, we use the gain metrics introduced in section 4.4, which will simplify the task of comparison between bins of STD and COUNT.

Table 6 shows spatial statistics for MB and Yanco divided in 3 ranges of STD (<0.03 m^3/m^3, 0.03-0.07 m^3/m^3, >0.07 m^3/m^3). Note that the total number of days analyzed drops drastically when STD or COUNT filtering is applied to spatial metrics. This is as expected since for a given time stamp, the samples have STD and COUNT values that belong to different bins and we need at least 5 samples in the same bin to compute statistics.. C4DIS SM dataset exhibits the lowest correlation (S and R) and the highest error (ubRMSD) with *in situ* when most of the pixels have high STD (>0.07 m^3/m^3). This seems plausible since large ubRMSD values can be produced by forcing events (rain, irrigation) in the 3-days window of DISPATCH, so the final SM_HR values would contain high uncertainty. We cannot generalize any behavior in performances for the medium and lower STD ranges (<0.07 m^3/m^3) since MB and Yanco show different trends. If we consider only Yanco, which is a much more homogeneous area in terms of climate and landscape properties, we can conclude that, regardless of the bias, the rest of spatial metrics are better as STD gets lower. Whether this is applicable to other homogeneous areas or not need to be the subject of additional studies.

Spatial statistics are also filtered for COUNT values (Table 7). In this respect, statistics are better for large values of COUNT (17-24 datasets). However, the number of days used in this computation is low (below 15) so the results may not be accurate.

Table 6- Spatial statistics as a function of the values of the STD dataset for MB and Yanco areas from 01/06/2010 to 31/05/2011. Best statistics are outlined and in italics. Last line of Yanco table has been crossed out because it refers to only one day of statistics.

	Yanco					**MB**				
STD	G_{EFFI}	G_{ACCU}	G_{ROBU}	G_{ubRMSD}	N_{days}	G_{EFFI}	G_{ACCU}	G_{ROBU}	G_{ubRMSD}	N_{days}
< 0.03	*0.27*	*0.24*	-0.22	*0.05*	11	0.15	*0.11*	-0.12	*-0.04*	45
0.03 - 0.07	0.13	0.06	*-0.11*	-0.10	39	*0.17*	0.05	-0.03	-0.07	108
> 0.7	~~**-0.47**~~	~~**-0.12**~~	~~**-0.42**~~	~~**-0.57**~~	~~**1**~~	-0.02	-0.09	*0.05*	-0.28	16

Table 7 - Spatial statistics as a function of the COUNT dataset for MB and Yanco areas from 01/06/2010 to 31/05/2011. Best statistics are outlined and in italics.

	Yanco					MB				
COUNT	G_{EFFI}	G_{ACCU}	G_{ROBU}	G_{ubRMSD}	N_{days}	G_{EFFI}	G_{ACCU}	G_{ROBU}	G_{ubRMSD}	N_{days}
1-8	0.16	0.08	-0.16	-0.16	69	0.16	0.07	*-0.05*	-0.11	143
9-16	0.12	0.16	-0.15	-0.07	22	0.14	-0.01	-0.12	-0.15	51
17-24	*0.44*	*0.29*	*-0.08*	*0.06*	11	*0.35*	*0.15*	-0.24	*-0.04*	13

Regarding the temporal domain, Yanco shows a deterioration of the metrics as STD increases (Table 8), which is consistent with the preliminary *in situ* spatial analysis and would be mainly due to the uncertainty added when precipitation or irrigation take place in the 3-days window of DISPATCH. Such trend is not revealed in the MB data (same table), and conclusions are difficult to be derived given the high heterogeneity within the network.

Concerning the COUNT dataset, Table 9 clearly shows that temporal statistics improve as COUNT increases. This seems to confirm that the methodology of averaging of the disaggregated ensemble helps to reduce random uncertainties in the temporal domain.

Table 8 - Temporal statistics as a function of the STD dataset for MB and Yanco areas from 01/06/2010 to 31/05/2011. Best statistics are outlined and in italics.

	Yanco					MB				
STD	G_{EFFI}	G_{ACCU}	G_{ROBU}	G_{ubRMSD}	$N_{samples}$	G_{EFFI}	G_{ACCU}	G_{ROBU}	G_{ubRMSD}	$N_{samples}$
< 0.025	*0.18*	*0.04*	-0.30	*-0.06*	472	*0.16*	0.03	-0.81	-0.06	904
0.025 - 0.040	0.04	-0.06	*-0.14*	-0.11	813	0.11	0.01	*0.03*	*-0.10*	1459
0.040 – 0.055	0.03	-0.04	-0.41	-0.18	192	0.13	*0.06*	-0.12	-0.03	475

Table 9 - Temporal statistics as a function of the COUNT dataset for MB and Yanco areas from 01/06/2010 to 31/05/2011. Best statistics are outlined and in italics.

	Yanco					MB				
COUNT	G_{EFFI}	G_{ACCU}	G_{ROBU}	G_{ubRMSD}	$N_{samples}$	G_{EFFI}	G_{ACCU}	G_{ROBU}	G_{ubRMSD}	$N_{samples}$
1-8	0.08	-0.06	-0.21	-0.15	965	0.14	0.02	0.08	-0.08	1910
9-16	0.17	-0.02	-0.18	-0.12	386	0.19	0.02	0.04	-0.09	737
17-24	*0.22*	*0.19*	*0.35*	*0.01*	126	*0.21*	*0.15*	*0.44*	*-0.03*	191

6. Conclusions

The C4DIS processor is the new SMOS L4 processor of the French ground segment CATDS, which provides global maps of disaggregated SM at 1 km resolution. The C4DIS processor is the operational version of the DISPATCH prototype (Merlin et al., 2012, 2013). DISPATCH disaggregates LR SM observations using HR soil temperature data. It models the physical link between soil temperature, evaporation and moisture with a semi-empirical SEE model and a first-order Taylor series expansion around the SM observation. The soil temperature is derived from the combination of LST, NDVI and elevation information. The C4DIS processor uses the SM dataset of the SMOS 1-day L3 CLF31A/D product from CATDS, the LST dataset of the MODIS MOD11A1 and MYD11A1 products from LP DAAC services, the NDVI dataset from the MOD13A2 product from LP DAAC services, and the elevation dataset from the GTOPO30 product from the USGS Eros Data Center.

In this study, the C4DIS products were evaluated for four different geographical areas: the Murrumbidgee validation network and the Yanco area for the period 06/2010 to 05/2011, and the Little Washita and Walnut Gulch networks for the period 01/2010 to 12/2014. The objective was to provide a first assessment of the processor under different climatic and land conditions. The performance was assessed by comparing the disaggregated (L4) and non-disaggregated (L3) SM datasets against the *in situ* measurements in both the spatial and temporal domains.. The *in situ* SM data was statistically analyzed beforehand in order to predict the suitability of the C4DIS processor for each area. We also evaluated the output COUNT and STD datasets as potential sources of information for quality assessment.

The evaluation of the disaggregated SM dataset in Murrumbidgee and Yanco brought results in coherence with previous versions of DISPATCH (Malbéteau et al., 2016b; Merlin et al., 2012), and presented improvements on the spatial correlation in the range 0.09-0.17. Similar enhancements were present in the temporal domain. Additionally, C4DIS SM maps succeeded to reveal spatial heterogeneities (rivers, irrigation areas, floods).

Little Washita and Walnut Gulch showed very low spatial metric values for both non-disaggregated and disaggregated SM fields, though disaggregation slightly improved the statistics. For the Little Washita, the scatter plots revealed that the performances were better in the dry section of the SM range (<0.15 m^3/m^3) and during summers, meaning that the improvement in spatial representation was possible under moisture-driven evaporation periods. Visual assessment of C4DIS SM maps showed that the disaggregated product was capable of revealing the presence of water bodies in the surrounding areas namely lakes.

For the Walnut Gulch network, the poor spatial correspondence with *in situ* was easily explained by the preliminary statistical analysis that we conducted on *in situ* SM data: this revealed very low spatial variability (mean spatial σ was equal to 0.03 m^3/m^3), which is one of the essential conditions for a good performance of the algorithm. The evaluation of this network brought to view that the algorithm needs to be improved to adapt to all types of soil. Although Walnut Gulch watershed also has a moisture-controlled evaporative profile (semi-arid to arid climate) like the Australian areas, the soil is mainly sandy with high infiltration rates, which obstructs the detection of surface SM variations by the algorithm.

When evaluating the temporal behavior of the (non-disaggregated and C4DIS) satellite SM series, we found an improvement of the slope of the regression line between C4DIS and the *in situ* data. The correlation was slightly hampered, especially in LW and WG, and the standard deviation of the differences also increased. This was likely to be caused by the increase in uncertainty associated with the use of multi-satellite data.

With the aim of making the C4DIS products useful in a global perspective, we evaluated how the other two output datasets, COUNT and STD, could help in the future definition of a quality flag. We showed that for a homogeneous area like Yanco, spatial and temporal metrics were better as STD decreased. Consistently, large COUNT values helped to decrease the random uncertainties and they improved temporal statistics. In this area, heterogeneity is mainly driven by precipitation and irrigation, and STD was directly linked to such events. On the contrary, STD and COUNT could not give sufficient information for quality control in more heterogeneous areas (like the entire Murrumbidgee), so we concluded that output C4DIS datasets must be combined with ancillary information like precipitation or other heterogeneity-related data sources to implement a good quality flag field.

In conclusion, the C4DIS processor performs well in regions with SM spatial variability mainly produced by external forcing agents (precipitation or irrigation). Additionally, the degree of variability must be enough so the application of a disaggregation technique is advisable. These two characteristics are mainly conditioned by the climate (semi-arid), soil properties (with moderate drainage), and land properties (low topography, quasi-homogeneous land cover). The proper performance of the processor can be predicted by looking at the *in situ* SM variability and assessing qualitatively the enounced characteristics. The C4DIS SM products can be evaluated by applying ordinary spatial and temporal statistics, visual inspection of maps as well as using the STD and COUNT datasets on homogeneous areas. In the future, including meteorological forcing (solar radiation, air temperature, wind speed and air humidity at 2 m; Stefan et al., 2015), precipitation (Djamai et al., 2015), soil texture (Merlin et al., 2016) and solar exposure (Malbéteau et al., 2016a) as ancillary data will help improve DISPATCH and elaborate a quality control dataset that will enlarge the applicability areas of the processor.

Acknowledgements

Initial setup and maintenance of the Murrumbidgee monitoring network used in this study was funded by the Australian Research Council (DP0343778, DP0557543) and by the CRC for Catchment Hydrology.

The MODIS products were retrieved from the online server http://e4ftl01.cr.usgs.gov/, courtesy of the NASA EOSDIS Land Processes Distributed Active Archive Center (LP DAAC), USGS/Earth Resources Observation and Science (EROS) Center, Sioux Falls, South Dakota.

The SMOS products were obtained from the Centre Aval de Traitement des Données SMOS (CATDS), operated for the "Centre National d'Etudes Spatiales" (CNES, France) by IFREMER (Brest, France).

This study was supported by the CNES “Terre, Océan, Surfaces Continentales, Atmosphère” program and by the French “Agence Nationale de la Recherche” MIXMOD-E project (ANR-13-JS06-0003-01).

Bibliography

Al Bitar, A., Leroux, D. J., Kerr, Y. H., Merlin, O., Richaume, P., Sahoo, A., & Wood, E. F. (2012). Evaluation of SMOS Soil Moisture Products Over Continental U.S. Using the SCAN / SNOTEL Network. *IEEE Transactions on Geoscience and Remote Sensing*, *50*(5), 1572–1586.

Albergel, C., Brocca, L., Wagner, W., de Rosnay, P., & Calvet, J. C. (2013). Selection of Performance Metrics for Global Soil Moisture Products: The Case of ASCAT Soil Moisture Product. In *Remote Sensing of Energy Fluxes and Soil Moisture Content* (pp. 431–448).

Albergel, C., de Rosnay, P., Gruhier, C., Muñoz-Sabater, J., Hasenauer, S., Isaksen, L., Kerr, Y. H., & Wagner, W. (2012). Evaluation of remotely sensed and modelled soil moisture products using global ground-based in situ observations. *Remote Sensing of Environment*, *118*, 215–226. doi:10.1016/j.rse.2011.11.017

Allen, P. B., & Naney, J. W. (1991). *Hydrology of the Little Washita River Watershed, Oklahoma: Data and Analyses*. United States Department of Agriculture, Agricultural Research Service, ARS-90.

Al-Yaari, A., Wigneron, J.-P., Ducharne, A., Kerr, Y. H., de Rosnay, P., de Jeu, R., Govind, A., Al Bitar, A., Albergel, C., Richaume, P., & Mialon, A. (2014). Global-scale evaluation of two satellite-based passive microwave soil moisture datasets (SMOS and AMSR-E) with respect to Land Data Assimilation System estimates. *Remote Sensing of Environment*, *149*, 181–195. doi:10.1016/j.rse.2014.04.006

Bindlish, R. (2015). Global Soil Moisture From the Aquarius/SAC-D Satellite: Description and Initial Assessment. *IEEE Geoscience and Remote Sensing Letters*, *12*(5), 923–927. doi:10.1109/LGRS.2014.2364151

Budyko, M. I. (1956). *Heat balance of the Earth's surface*. Leningrad.

Carlson, T. N. (2007). An Overview of the "Triangle Method" for Estimating Surface Evapotranspiration and Soil Moisture from Satellite Imagery. *Sensors*, *7*(8), 1612–1629. doi:10.3390/s7081612

Carlson, T. N., Gillies, R. R., & Perry, E. M. (1994). A method to make use of thermal infrared temperature and NDVI measurements to infer surface soil water content and fractional vegetation cover. *Remote Sensing Reviews*. doi:10.1080/02757259409532220

Chauhan, N. S., Miller, S., & Ardanuy, P. (2003). Spaceborne soil moisture estimation at high resolution: a microwave-optical/IR synergistic approach. *International Journal of Remote Sensing*, *24*(22), 4599–4622. doi:10.1080/0143116031000156837

Chen, F., Crow, W. T., Starks, P. J., & Moriasi, D. N. (2011). Improving hydrologic predictions of a catchment model via assimilation of surface soil moisture. *Advances in Water Resources*, *34*(4), 526–536. doi:10.1016/j.advwatres.2011.01.011

Cosh, M. H., Jackson, T. J., Bindlish, R., & Prueger, J. H. (2004). Watershed scale temporal and spatial stability of soil moisture and its role in validating satellite estimates. *Remote Sensing of Environment*, *92*, 427–435. doi:10.1016/j.rse.2004.02.016

Cosh, M. H., Jackson, T. J., Moran, S., & Bindlish, R. (2008). Temporal persistence and stability of surface soil moisture in a semi-arid watershed. *Remote Sensing of Environment*, *112*(2), 304–313. doi:10.1016/j.rse.2007.07.001

Cosh, M. H., Jackson, T. J., Starks, P. J., & Heathman, G. (2006). Temporal stability of surface soil moisture in the Little Washita River watershed and its applications in satellite soil moisture product validation. *Journal of Hydrology*, *323*(1-4), 168–177. doi:10.1016/j.jhydrol.2005.08.020

Daly, E., & Porporato, A. (2005). A Review of Soil Moisture Dynamics: From Rainfall Infiltration to Ecosystem Response. *Environmental Engineering Science*. doi:10.1089/ees.2005.22.9

Das, N. N., Entekhabi, D., & Njoku, E. G. (2011). An algorithm for merging SMAP radiometer and radar data for high-resolution soil-moisture retrieval. *IEEE Transactions on Geoscience and Remote Sensing*, *49*(5), 1504–1512. doi:10.1109/TGRS.2010.2089526

Das, N. N., Entekhabi, D., Njoku, E. G., Shi, J. J. C., Johnson, J. T., & Colliander, A. (2014). Tests of the SMAP combined radar and radiometer algorithm using airborne field campaign observations and simulated data. *IEEE Transactions on Geoscience and Remote Sensing*, *52*(4), 2018–2028. doi:10.1109/TGRS.2013.2257605

Delwart, S., Bouzinac, C., Wursteisen, P., Berger, M., Drinkwater, M., Martín-Neira, M., & Kerr, Y. H. (2008). SMOS validation and the COSMOS campaigns. *IEEE Transactions on Geoscience and Remote Sensing*, *46*(3), 695–703. doi:10.1109/TGRS.2007.914811

Dirmeyer, P. A. (2000). Using a global soil wetness dataset to improve seasonal climate simulation. *J. Climate*, (13), 2900–2922.

Djamai, N., Magagi, R., Goïta, K., Merlin, O., Kerr, Y. H., & Roy, A. (2015). Downscaling satellite-based soil moisture for cloudy days using the DISPATCH algorithm and CLASS land surface scheme. *Submitted Remote Sensing of Environment*.

Douville, H. (2004). Relevance of soil moisture for seasonal atmospheric predictions: Is it an initial value problem? *Climate Dynamics*, *22*(4), 429–446. doi:10.1007/s00382-003-0386-5

Draper, C., Reichle, R. H., De Lannoy, G. J. M., & Liu, Q. (2012). Assimilation of passive and active microwave soil moisture retrievals. *Geophysical Research Letters*, *39*(4). doi:10.1029/2011GL050655

Drusch, M. (2007). Initializing numerical weather prediction models with satellite-derived surface soil moisture: Data assimilation experiments with ECMWF’s integrated forecast system and the TMI soil moisture data set. *Journal of Geophysical Research: Atmospheres*, *112*(3). doi:10.1029/2006JD007478

Entekhabi, D., Njoku, E. G., O’Neill, P. E., Kellogg, K. H., Crow, W. T., Edelstein, W. N., … Van Zyl, J. (2010a). The soil moisture active passive (SMAP) mission. *Proceedings of the IEEE*, *98*(5), 704–716. doi:10.1109/JPROC.2010.2043918

Entekhabi, D., Reichle, R. H., Koster, R. D., & Crow, W. T. (2010b). Performance Metrics for Soil Moisture Retrievals and Application Requirements. *Journal of Hydrometeorology*, *11*, 832–840. doi:10.1175/2010JHM1223.1

Fang, B., Lakshmi, V., Bindlish, R., Jackson, T. J., Cosh, M. H., & Basara, J. (2013). Passive Microwave Soil Moisture Downscaling Using Vegetation Index and Skin Surface Temperature. *Vadose Zone Journal*, *12*(3), 0. doi:10.2136/vzj2013.05.0089

Guérif, M., & Duke, C. . (2000). Adjustment procedures of a crop model to the site specific characteristics of soil and crop using remote sensing data assimilation. *Agriculture, Ecosystems & Environment*. doi:10.1016/S0167-8809(00)00168-7

Jackson, T. J., Bindlish, R., Cosh, M. H., Zhao, T., Starks, P. J., Bosch, D. D., Seyfried, M., Moran, M. S., Goodrich, D. C., Kerr, Y. H., & Leroux, D. J. (2012). Validation of soil moisture and Ocean Salinity (SMOS) soil moisture over watershed networks in the U.S. *IEEE Transactions on Geoscience and Remote Sensing*, *50*(5), 1530–1543. doi:10.1109/TGRS.2011.2168533

Jackson, T. J., Cosh, M. H., Bindlish, R., Starks, P. J., Bosch, D. D., Seyfried, M., Goodrich, D. C., Moran, M. S., & Du, J. (2010). Validation of advanced microwave scanning radiometer soil moisture products. *IEEE Transactions on Geoscience and Remote Sensing*, *48*(12), 4256–4272. doi:10.1109/TGRS.2010.2051035

Jiang, L., & Islam, S. (2003). An intercomparison of regional latent heat flux estimation using remote sensing data. *International Journal of Remote Sensing*. doi:10.1080/01431160210154821

Kerr, Y. H., Berthon, L., Mialon, A., Cabot, F., Al Bitar, A., Richaume, P., Leroux, D. J., Bircher, S., Lawrence, H., Quesney, A., & Jacquette, E. (2014). *CATDS LEVEL 3 - Data product description - Soil Moisture and Brightness Temperature*.

Kerr, Y. H., Jacquette, E., Al Bitar, A., Cabot, F., Mialon, A., & Richaume, P. (2013). *CATDS SMOS L3 soil moisture retrieval processor, Algorithm Theoretical Baseline Document (ATBD)*.

Kerr, Y. H., & Njoku, E. G. (1990). Semiempirical model for interpreting microwave emission from semiarid land surfaces as seen from space. *IEEE Transactions on Geoscience and Remote Sensing*, *28*(3), 384–393. doi:10.1109/36.54364

Kerr, Y. H., Waldteufel, P., Richaume, P., Wigneron, J.-P., Ferrazzoli, P., Mahmoodi, A., Al Bitar, A., Cabot, F., Gruhier, C., Juglea, S. E., Leroux, D. J., Mialon, A., & Delwart, S. (2012). The SMOS Soil Moisture Retrieval Algorithm. *Geoscience and Remote Sensing*, *50*(5), 1384–1403.

Kerr, Y. H., Waldteufel, P., Wigneron, J.-P., Delwart, S., Cabot, F., Boutin, J., Escorihuela, M.-J., Font, J., Reul, N., Gruhier, C., Juglea, S. E., Drinkwater, M., Hahne, A., Martin-Neira, M., & Mecklenburg, S. (2010). The SMOS Mission: New Tool for Monitoring Key Elements of the Global Water Cycle. *Proceedings of the IEEE*, *98*(5), 666–687. doi:10.1109/JPROC.2010.2043032

Kerr, Y. H., Waldteufel, P., Wigneron, J.-P., Martinuzzi, J. M., Font, J., & Berger, M. (2001). Soil moisture retrieval from space: The Soil Moisture and Ocean Salinity (SMOS) mission. *IEEE Transactions on Geoscience and Remote Sensing*, *39*(8), 1729–1735. doi:10.1109/36.942551

Kim, J., & Hogue, T. S. (2012). Improving spatial soil moisture representation through integration of AMSR-E and MODIS products. *IEEE Transactions on Geoscience and Remote Sensing*, *50*(2), 446–460. doi:10.1109/TGRS.2011.2161318

Laio, F., Porporato, A., Ridolfi, L., & Rodríguez-Fernández, N. J. (2002). On the seasonal dynamics of mean soil moisture. *Journal of Geophysical Research: Atmospheres*. doi:10.1029/2001JD001252

Leroux, D. J., Kerr, Y. H., Al Bitar, A., Bindlish, R., Jackson, T. J., Berthelot, B., & Portet, G. (2013). Comparison Between SMOS, VUA, ASCAT, and ECMWF Soil Moisture Products Over Four Watersheds in U.S. *IEEE Transactions on Geoscience and Remote Sensing*, *52*(3), 1–10.

Lievens, H., Tomer, S. K., Al Bitar, A., De Lannoy, G. J. M., Drusch, M., Dumedah, G., Hendricks Franssen, H.-J., Kerr, Y. H., Martens, B., Pan, M., Roundy, J. K., Vereecken, H., Walker, J. P., Wood, E. F., Verhoest, N. E. C., & Pauwels, V. R. N. (2015). SMOS soil moisture assimilation for improved hydrologic simulation in the Murray Darling Basin, Australia. *Remote Sensing of Environment*, *168*, 146–162. doi:10.1016/j.rse.2015.06.025

Malbéteau, Y., Merlin, O., Gascoin, S., Gastellu, J. P., Olivera, L., Mattar, C., & Khabba, S. (2016a). Correcting land surface temperature data for elevation and illumination effects in mountainous areas: a case study using ASTER data over the Imlil valley, Morocco. *Submitted to Remote Sensing of Environment.*

Malbéteau, Y., Merlin, O., Molero, B., Rüdiger, C., & Bacon, S. (2016b). DisPATCh as a tool to evaluate coarse-scale remotely sensed soil moisture using localized in situ measurements: Application to {SMOS} and AMSR-E data in Southeastern Australia. *International Journal of Applied Earth Observation and Geoinformation*, *45, Part B*, 221–234. doi:http://dx.doi.org/10.1016/j.jag.2015.10.002

Manabe, S. (1969). Climate and the ocean circulation. I. The atmospheric circulation and the hydrology of the Earth's surface. *Monthly Weather Review, 97(11)*, 739–774.

Merlin, O., Al Bitar, A., Walker, J. P., & Kerr, Y. H. (2009). A sequential model for disaggregating near-surface soil moisture observations using multi-resolution thermal sensors. *Remote Sensing of Environment*, *113*(10), 2275–2284. doi:10.1016/j.rse.2009.06.012

Merlin, O., Al Bitar, A., Walker, J. P., & Kerr, Y. H. (2010a). An improved algorithm for disaggregating microwave-derived soil moisture based on red, near-infrared and thermal-infrared data. *Remote Sensing of Environment*, *114*(10), 2305–2316. doi:10.1016/j.rse.2010.05.007

Merlin, O., Chehbouni, A., Boulet, G., & Kerr, Y. H. (2006). Assimilation of Disaggregated Microwave Soil Moisture into a Hydrologic Model Using Coarse-Scale Meteorological Data. *Journal of Hydrometeorology*. doi:10.1175/JHM552.1

Merlin, O., Duchemin, B., Hagolle, O., Jacob, F., Coudert, B., Chehbouni, G., Dedieu, G., Garatuza, J., & Kerr, Y. H. (2010b). Disaggregation of MODIS surface temperature over an agricultural area using a time series of Formosat-2 images. *Remote Sensing of Environment, 114*(11), 2500–2512. doi:10.1016/j.rse.2010.05.025

Merlin, O., Escorihuela, M.-J., Mayoral, M. A., Hagolle, O., Al Bitar, A., & Kerr, Y. H. (2013). Self-calibrated evaporation-based disaggregation of SMOS soil moisture: An evaluation study at 3 km and 100 m resolution in Catalunya, Spain. *Remote Sensing of Environment*, *130*(2013), 25–38.

Merlin, O., Malbéteau, Y., Notfi, Y., Bacon, S., Er-raki, S., Khabba, S., & Jarlan, L. (2015). Performance metrics for soil moisture downscaling methods: Application to DISPATCH data in central Morocco. *Remote Sensing, 7*(4), 3783–3807. doi:10.3390/rs70403783

Merlin, O., Rüdiger, C., Al Bitar, A., Richaume, P., Walker, J. P., & Kerr, Y. H. (2012). Disaggregation of SMOS Soil Moisture in Southeastern Australia. *IEEE Transactions on Geoscience and Remote Sensing*, *50*(5), 1556–1571. doi:10.1109/TGRS.2011.2175000

Merlin, O., Rüdiger, C., Richaume, P., Al Bitar, A., Mialon, A., Walker, J. P., & Kerr, Y. H. (2010c). Disaggregation as a top-down approach for evaluating 40 km resolution SMOS data using point-scale measurements: application to AACES-1. *Remote Sensing for Agriculture, Ecosystems, and Hydrology Xii*, *7824*, -\r666. doi:Artn 78240i\rDoi 10.1117/12.865751

Merlin, O., Stefan, V. G., Amazirh, A., Chanzy, A., Ceschia, E., Tallec, T., Beringer, J., Gentine, P., Er-Raki, S., Bircher, S., & Khabba, S. (2016). Modeling soil evaporation efficiency in a range of soil and atmospheric conditions: A downward approach based on multi-site data. *Submitted to Water Resources Research*.

Merlin, O., Walker, J. P., Chehbouni, A., & Kerr, Y. H. (2008). Towards deterministic downscaling of SMOS soil moisture using MODIS derived soil evaporative efficiency. *Remote Sensing of Environment*, *112*(10), 3935–3946. doi:10.1016/j.rse.2008.06.012

Mladenova, I., Lakshmi, V., Jackson, T. J., Walker, J. P., Merlin, O., & de Jeu, R. A. M. (2011). Validation of AMSR-E soil moisture using L-band airborne radiometer data from National Airborne Field Experiment 2006. *Remote Sensing of Environment*, *115*(8), 2096–2103. doi:10.1016/j.rse.2011.04.011

Mood, A. M., Graybill, F. A., & Boes, D. C. (1974). *Introduction to the Theory of Statistics*. *McGrawHill series in probability and statistics* (Vol. 3). Retrieved from http://www.librarything.com/work/1154157/book/32217714

Moran, M. S., Clarke, T. R., Inoue, Y., & Vidal, A. (1994). Estimating crop water deficit using the relation between surface-air temperature and spectral vegetation index. *Remote Sensing of Environment*. doi:10.1016/0034-4257(94)90020-5

Narayan, U., Lakshmi, V., & Jackson, T. J. (2006). High-resolution change estimation of soil moisture using L-band radiometer and radar observations made during the SMEX02 experiments. *IEEE Transactions on Geoscience and Remote Sensing*, *44*(6), 1545–1554. doi:10.1109/TGRS.2006.871199

Njoku, E. G., & Entekhabi, D. (1996). Passive microwave remote sensing of soil moisture. *Journal of Hydrology*. doi:10.1016/0022-1694(95)02970-2

Noilhan, J., & Planton, S. (1989). A simple parameterization of land surface processes for meteorological models. *Monthly Weather Review*, *117*(3), 536–549.

Oliva, R., Daganzo-Eusebio, E., Kerr, Y. H., Mecklenburg, S., Nieto, S., Richaume, P., & Gruhier, C. (2012). SMOS radio frequency interference scenario: Status and actions taken to improve the RFI environment in the 1400-1427-MHZ passive band. *IEEE Transactions on Geoscience and Remote Sensing*, *50*(5 PART 1), 1427–1439. doi:10.1109/TGRS.2012.2182775

Panciera, R., Walker, J. P., Jackson, T. J., Gray, D. a., Tanase, M. a., Ryu, D., Monerris, A., Yardley, H., Rüdiger, C., Wu, X., Gao, Y., & Hacker, J. M. (2014). The soil moisture active passive experiments (SMAPEx): Toward soil moisture retrieval from the SMAP mission. *IEEE Transactions on Geoscience and Remote Sensing*, *52*(1), 490–507. doi:10.1109/TGRS.2013.2241774

Peischl, S., Walker, J. P., Rüdiger, C., Ye, N., Kerr, Y. H., Kim, E., Bandara, R., & Allahmoradi, M. (2012). The AACES field experiments: SMOS calibration and validation across the Murrumbidgee River catchment. *Hydrology and Earth System Sciences*, *16*(6), 1697–1708. doi:10.5194/hess-16-1697-2012

Piles, M., Camps, A., Vall-Llossera, M., Corbella, I., Panciera, R., Rüdiger, C., Kerr, Y. H., & Walker, J. P. (2011). Downscaling SMOS-derived soil moisture using MODIS visible/infrared data. *IEEE Transactions on Geoscience and Remote Sensing*, *49*(9), 3156–3166. doi:10.1109/TGRS.2011.2120615

Rodgers, J. L., & Nicewander, W. A. (1988). Thirteen ways to look at the correlation coefficient. *The American Statistician*, *42*(1), 59–66.

Salkind, N. J. (2010). Standard error of the estimate. In SAGE (Ed.), *Encyclopedia of research design. Volume 3* (pp. 1426–1430). London.

Schmugge, T. J. (1998). Applications of passive microwave observations of surface soil moisture. *Journal of Hydrology*, *212-213*(1-4), 188–197. doi:10.1016/S0022-1694(98)00209-1

Smith, A. B., Walker, J. P., Western, A. W., Young, R. I., Ellett, K. M., Pipunic, R. C., Grayson, R. B., Siriwardena, L., Chiew, F. H. S., & Richter, H. (2012). The Murrumbidgee soil moisture monitoring network data set. *Water Resour. Res.*, *48*(7), W07701. doi:10.1029/2012WR011976

Solano, R., Didan, K., Jacobson, A., & Huete, A. (2010). *MODIS Vegetation Index User's Guide (MOD13 Series)* (Vol. v2.0).

Stefan, V. G., Merlin, O., Er-Raki, S., Escorihuela, M.-J., & Khabba, S. (2015). Consistency between in situ, model-derived and image-based soil temperature endmembers: towards a robust data-based model for multi-resolution monitoring of crop evapotranspiration. *Remote Sensing*, *7*(8), 10444–10479.

Walker, J. P., & Houser, P. R. (2004). Requirements of a global near-surface soil moisture satellite mission: Accuracy, repeat time, and spatial resolution. *Advances in Water Resources*, *27*(8), 785–801. doi:10.1016/j.advwatres.2004.05.006

Wan, Z. (1999). *MODIS Land-Surface Temperature Algorithm Theoretical Basis Document (LST ATBD)*.

Wan, Z. (2006). *MODIS Land Surface Temperature Products Users' Guide - Collection 5*. Sioux Falls, South Dakota,. Retrieved from http://www.icess.ucsb.edu/modis/LstUsrGuide/MODIS_LST_products_Users_guide_C5.pdf

Wanders, N., Bierkens, M., de Jong, S. M., de Roo, A., & Karssenberg, D. (2014). The benefits of using remotely sensed soil moisture in parameter identification of large-scale hydrological models. *Water Resources Research*, *50*(8), 6874–6891. doi:10.1002/2013WR014639

Wigneron, J.-P., Kerr, Y. H., Waldteufel, P., Saleh, K., Escorihuela, M.-J., Richaume, P., Ferrazzoli, P., de Rosnay, P., Gurney, R., Calvet, J.-C., Grant, J. P., Guglielmetti, M., Hornbuckle, B., Mätzler, C., Pellarin, T., & Schwank, M. (2007). L-band Microwave Emission of the Biosphere (L-MEB) Model: Description and calibration against experimental data sets over crop fields. *Remote Sensing of Environment*, *107*, 639–655. doi:10.1016/j.rse.2006.10.014

Zhan, X., Houser, P. R., Walker, J. P., & Crow, W. T. (2006). A method for retrieving high-resolution surface soil moisture from hydros L-band radiometer and radar observations. *IEEE Transactions on Geoscience and Remote Sensing*, *44*(6), 1534–1544. doi:10.1109/TGRS.2005.863319

List of figures